INSTITUTE OF PLASMA PHYSICS
OF THE CZECH ACADEMY OF SCIENCES

Fast Spectroscopy of nanosecond plasmas in liquids: the quest for signatures of direct, bubble-assisted and bubble-driven discharge mechanisms

M. Šimek

Online Low Temperature Plasma (OLTP) seminar, May 17, 2022

IPP

DISCHARGES WITH LIQUIDS

Chemistry & physics of plasma-liquid interactions and environ-mental, biological/ biomedical, chemical applications (water pollution control, plasma medicine, organic synthesis).

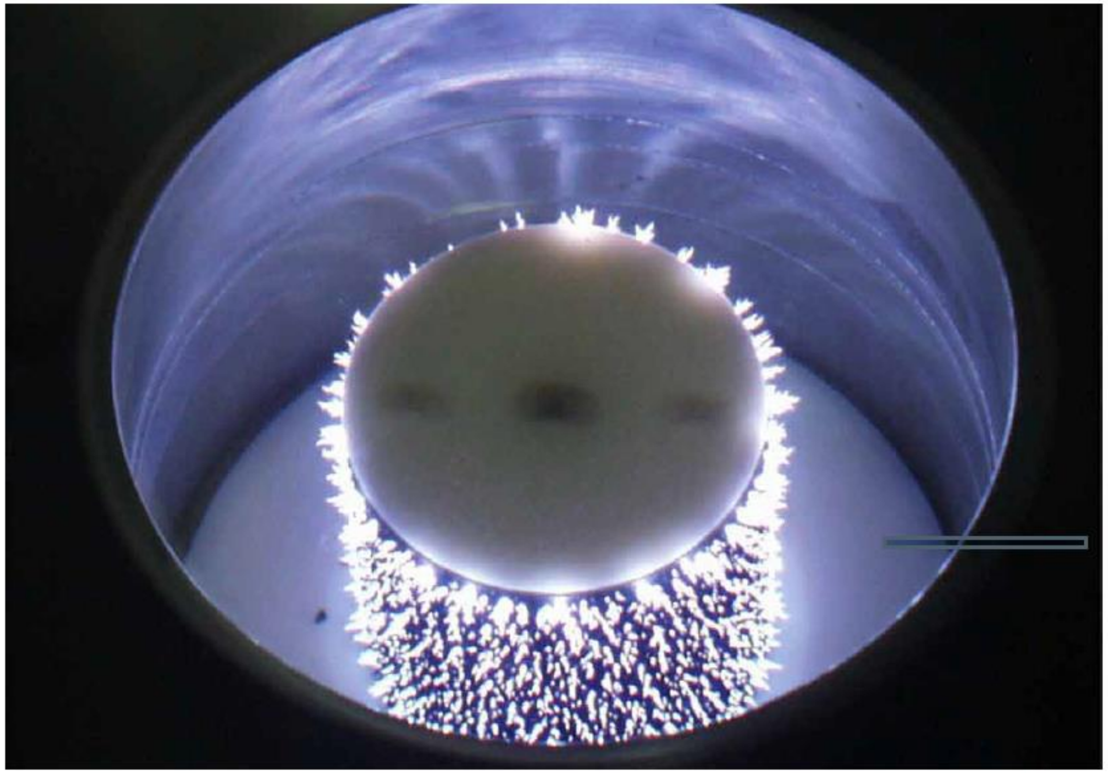

Multichannel discharges in water using porous ceramic-coated electrodes

DISCHARGES IN GASES

Physics, kinetics & chemistry of gaseous streamer discharges, various environmental and biological/biomedical applications (ozone generation, surface treatment, plasma medicine).

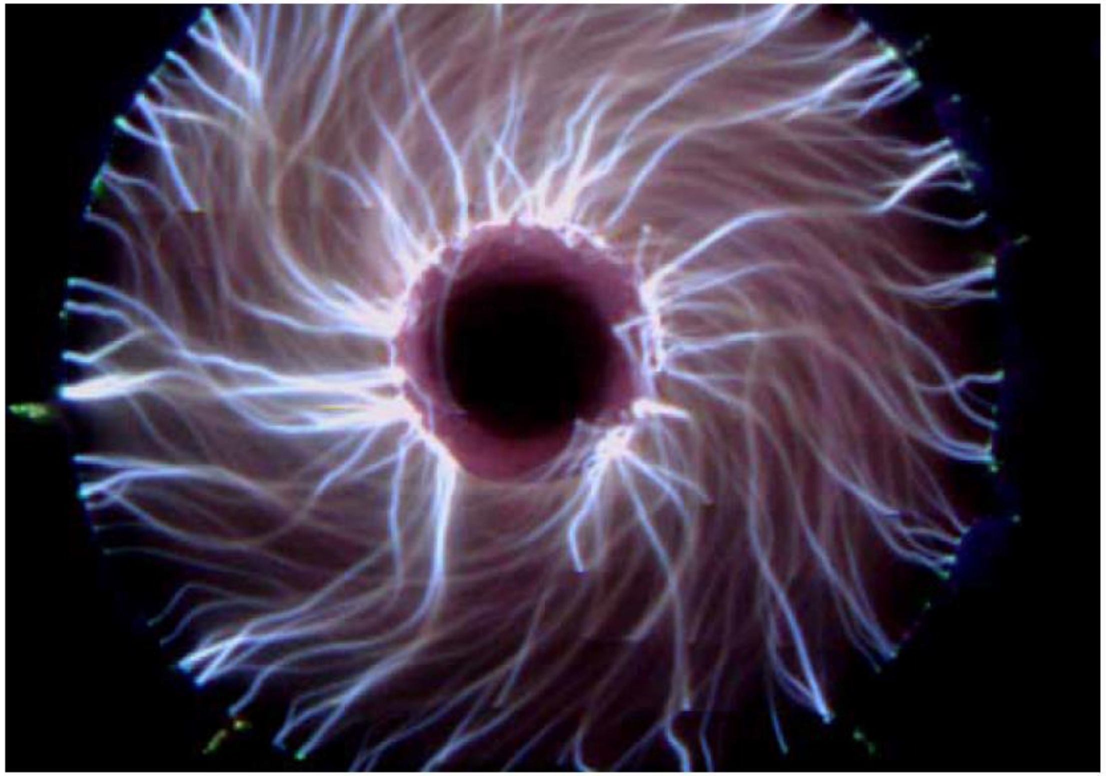

Surface AC DBD streamer discharges in air

GENERAL MOTIVATION

- Biomedical applications & plasma agriculture
- Reactive species, discharge induced chemistry in liquids
- Mechanism(s) of discharge initiation in liquid H_2O
- Discharge diagnostics

Streamer discharges in water

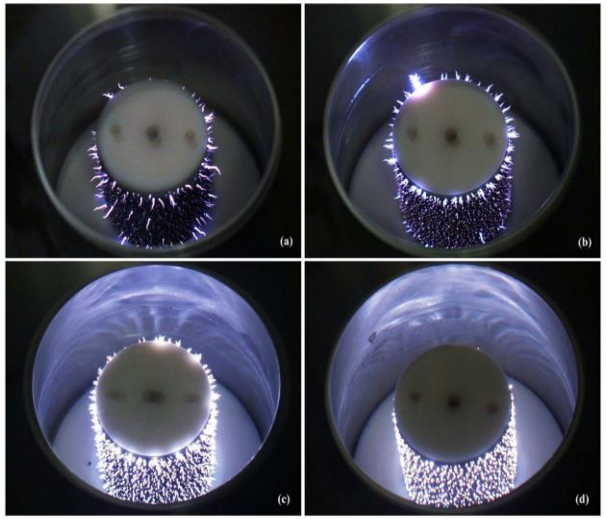

Multichannel discharges in water

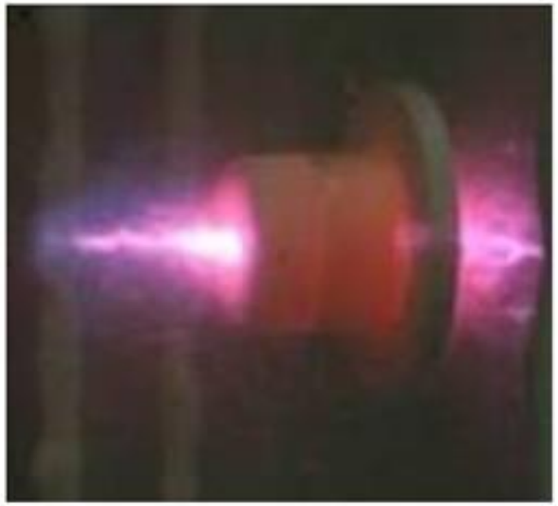

Discharges in vapor bubbles in water

Discharges in contact with water surface

MECHANISMS OF DISCHARGE INITIATION IN LIQUID WATER

Bubble-driven breakdown

- Long rise-time of high voltage waveform
- Mechanism: **Joule heating creates vapor bubbles, where the discharge is initiated.**

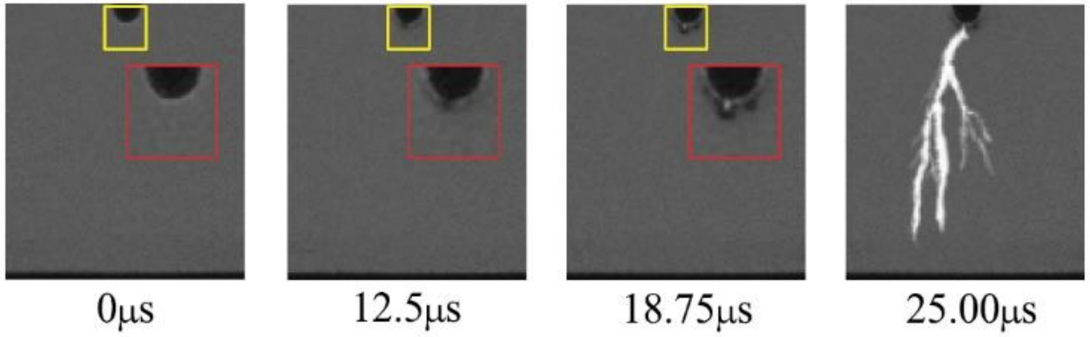

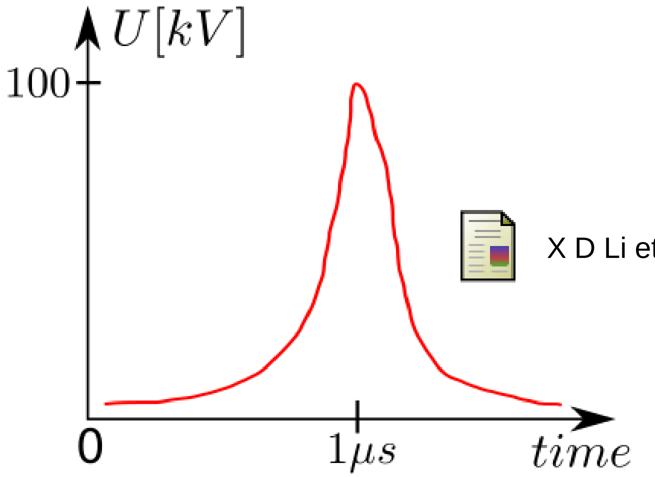

X D Li et al 2017 J. Phys. D: Appl. Phys. 50 255301

Direct breakdown

- ns rise-time of high voltage waveform
- Joule heating is impossible on such a short timescale
- Mechanism: ????

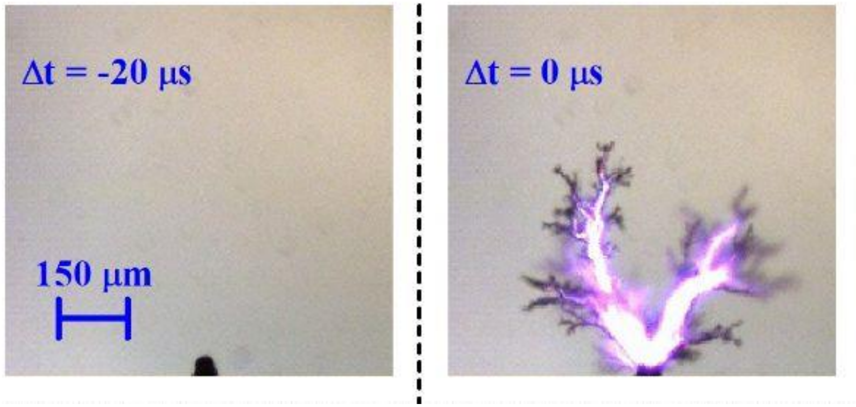

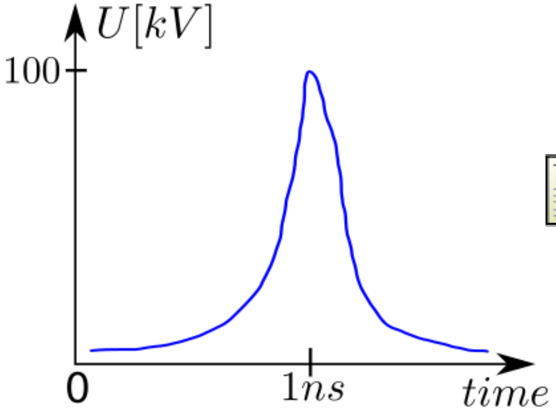

Petr Hoffer *et al* 2022 *Plasma Sources Sci. Technol.* **31** 015005

MECHANISMS OF DISCHARGE INITIATION IN LIQUID WATER

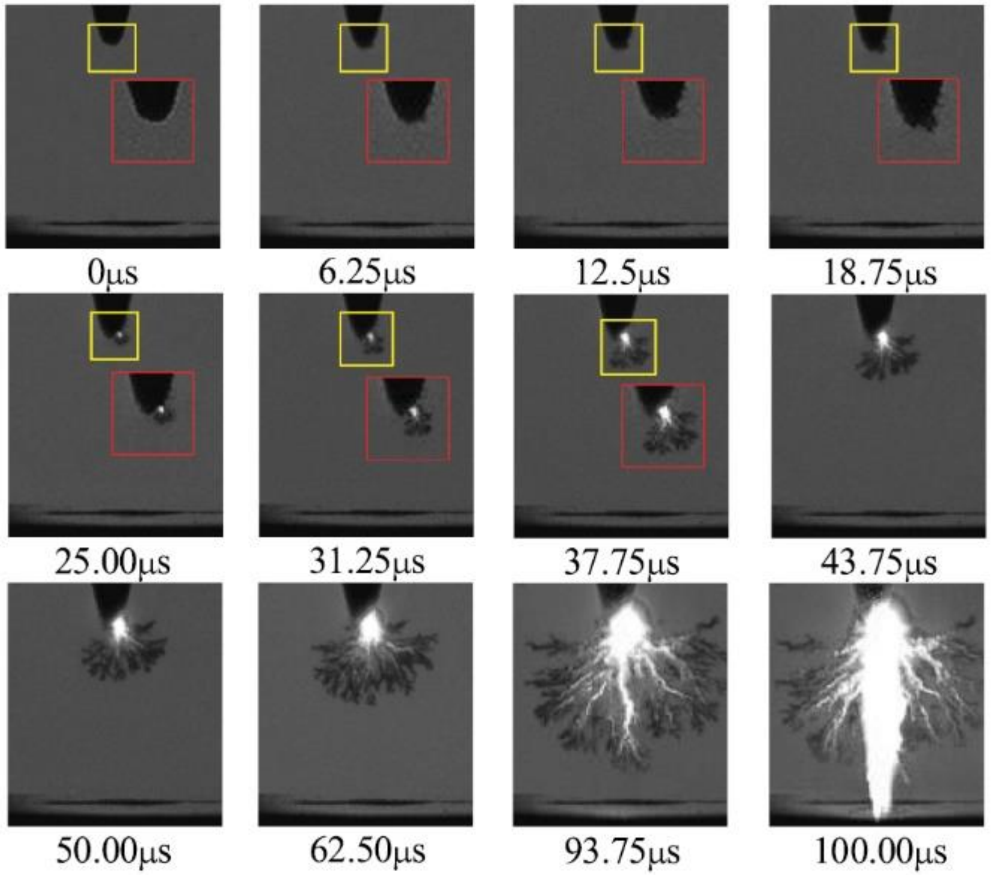

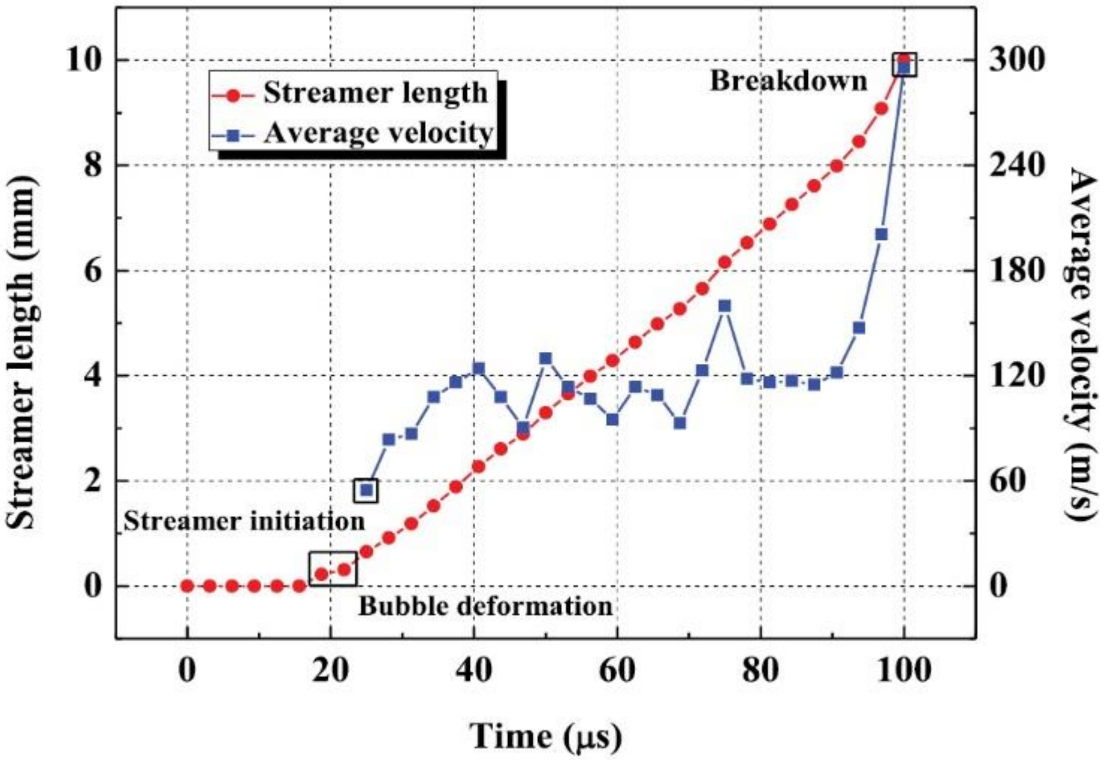

X D Li et al 2017 J. Phys. D: Appl. Phys. 50 255301

MECHANISMS OF DISCHARGE INITIATION IN LIQUID WATER

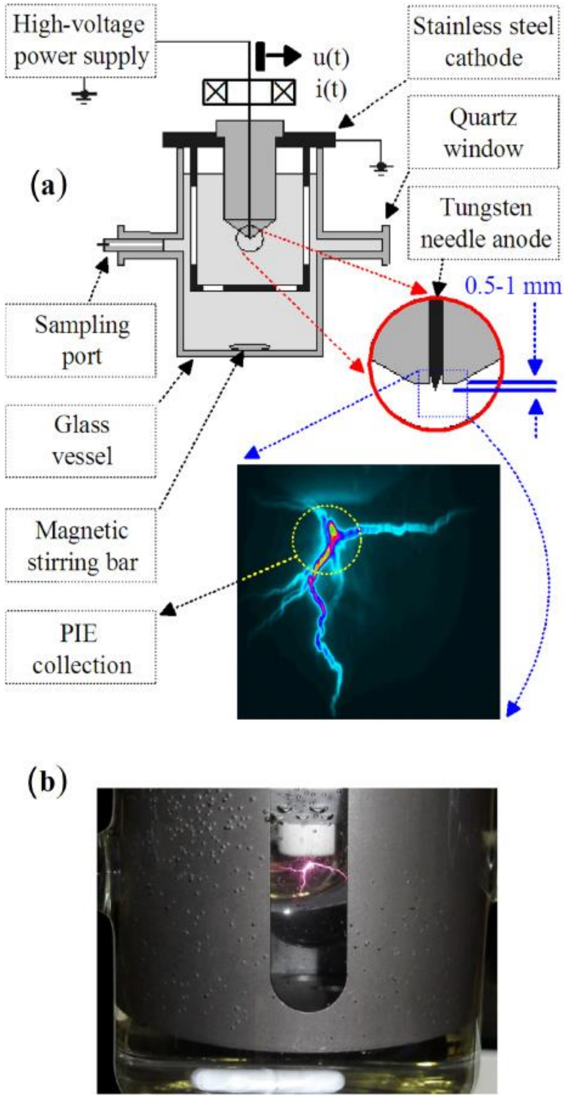

- usually one primary filament with 4-6 branches developing during the HV pulse
- complex UV-vis-NIR emission spectrum

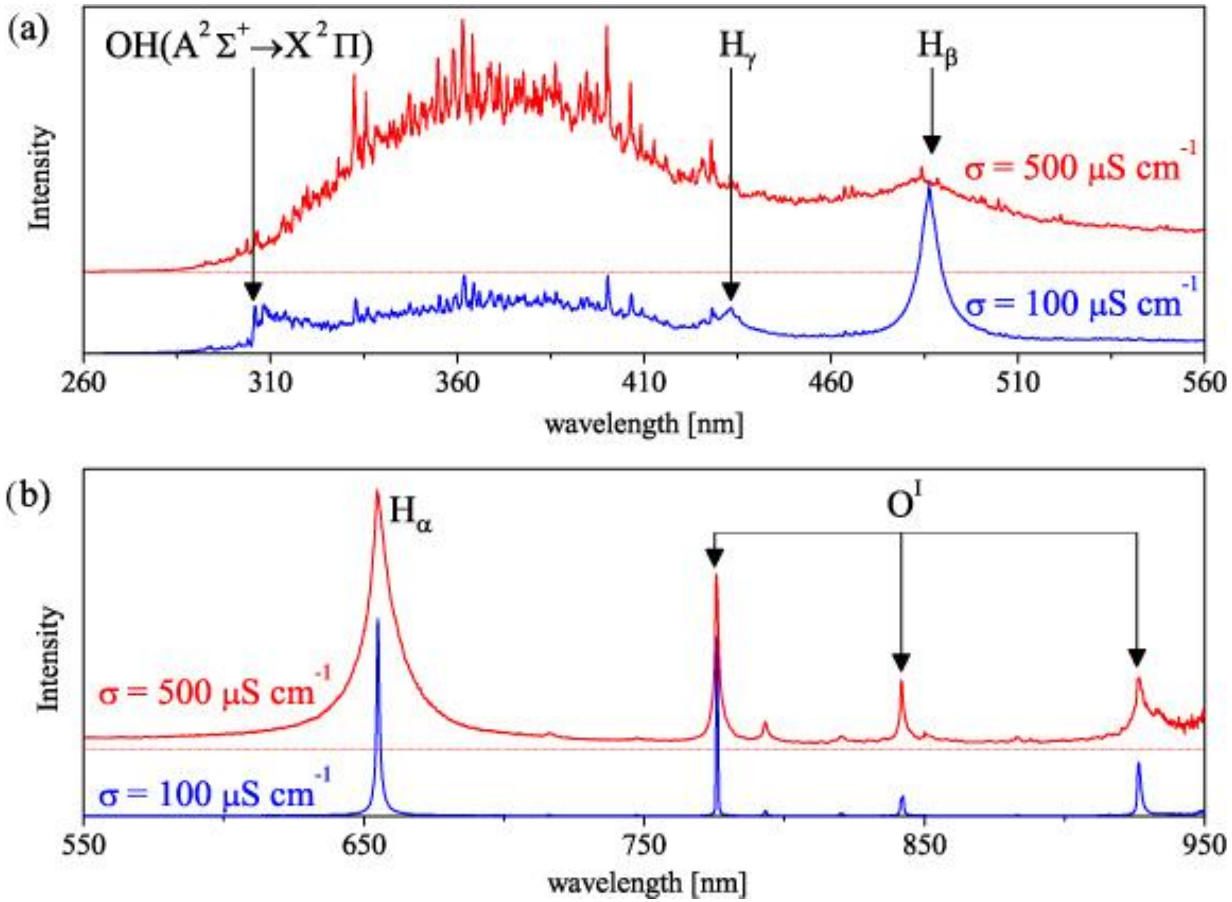

Šimek et al. 2012 *Plasma Sources Sci. Technol.* **21** 055031

MECHANISMS OF DISCHARGE INITIATION IN LIQUID WATER

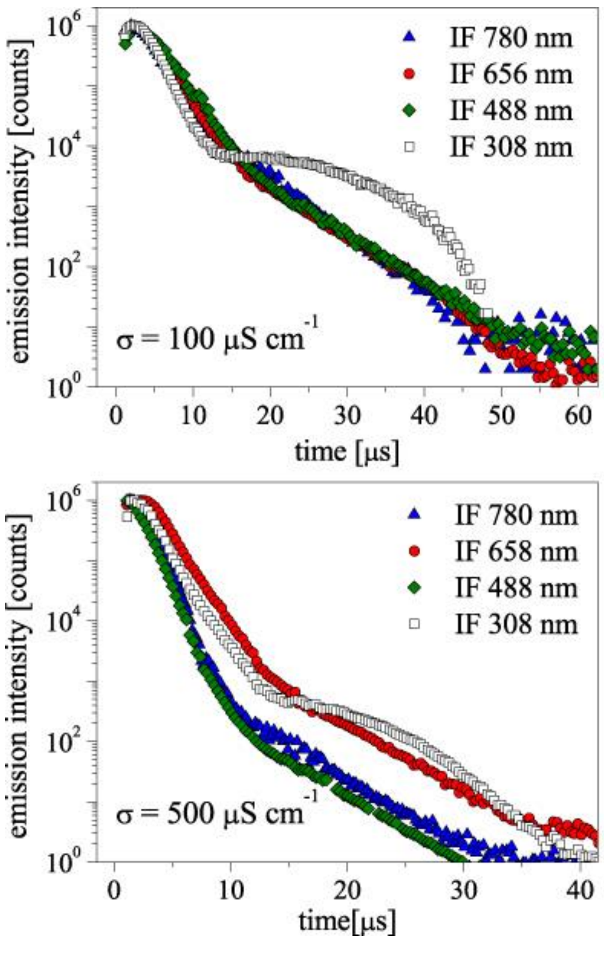

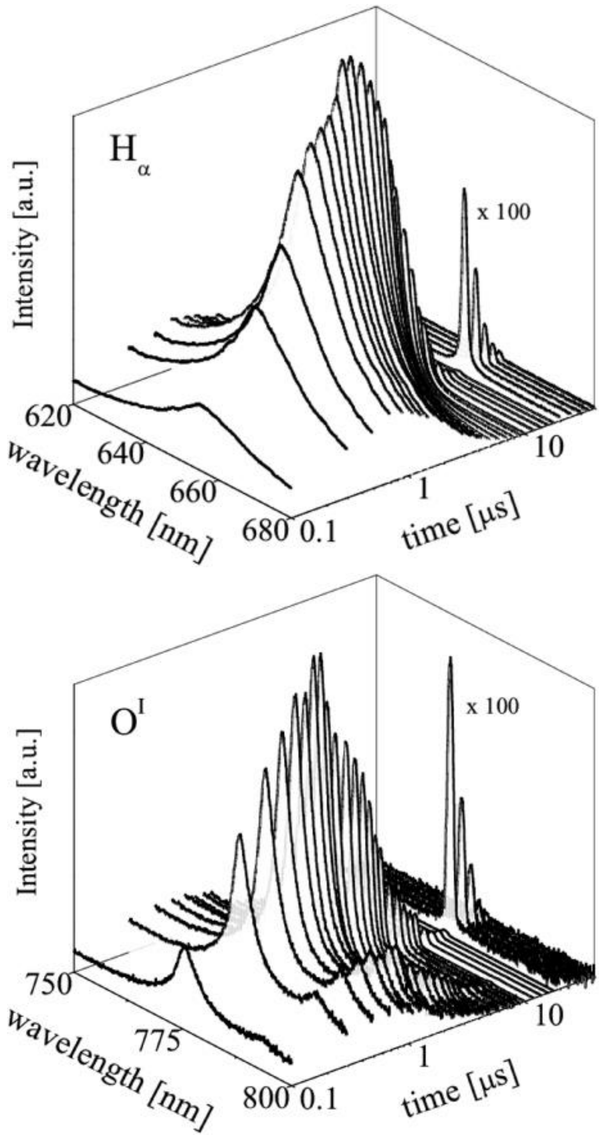

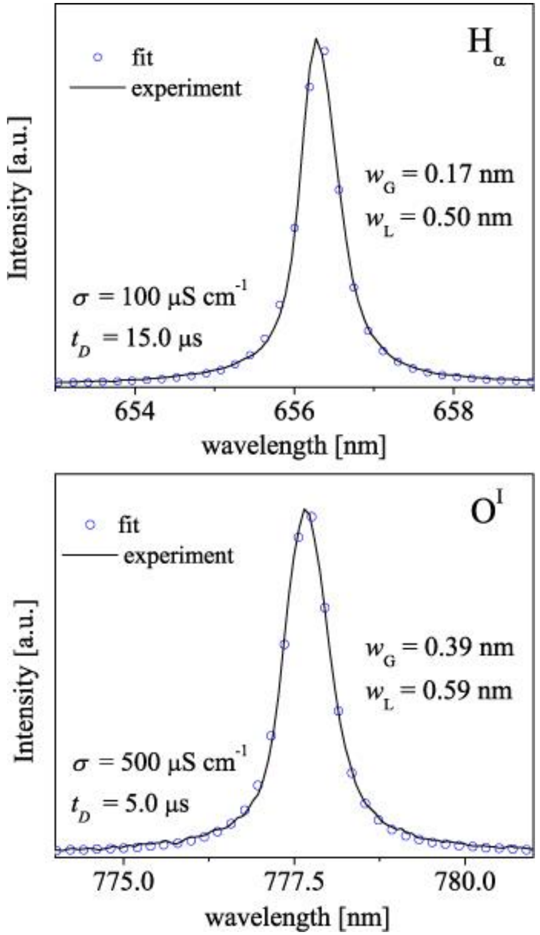

Šimek et al. 2012 *Plasma Sources Sci. Technol.* **21** 055031

MECHANISMS OF DISCHARGE INITIATION IN LIQUID WATER

- Liquid water … associated liquids … hydrogen bonding
- H-bond = mainly electrostatic attraction between H atom (which is covalently bound to a more electronegative atom) and an atom or a group of atoms in the same or a different molecule (O atom in case of H_2O
- H-bond is stronger than van der Waals but weaker than fully covalent bonds
- Typical length of H-bond 0.2A, average lifetime few ps
- Each H_2O can be H-bonded with up to 4 other H_2O molecules

Liu et.al.2018 *Chem. Sci.* **9** 2065

ab initio molecular dynamics simulation of liquid water

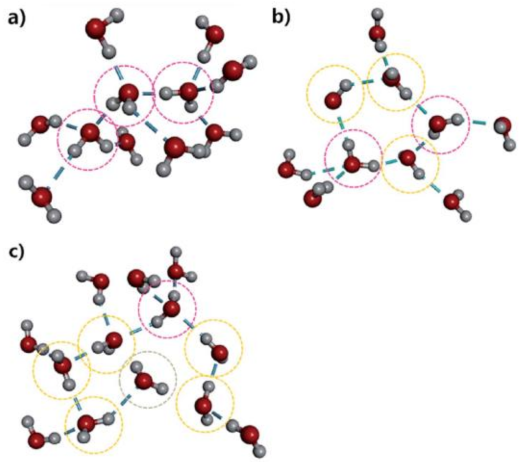

Fig. 4 The representative hydrogen-bond structures in the simulated liquid water. The dashed line denotes the hydrogen-bond. The pink, yellow and grey circles label the double-donor (DD), single-donor (SD) and none-donor (ND) configurations of the hydrogen-bonded water molecules, respectively.

Dynamical picture of liquid water: The hydrogen-bond switching dynamics in liquid water are very fast, with a hydrogen-bond life time of around 0.78 ps

Water microstructure: A dynamical mixture of tetrahedral and "ring-and-chain"- like structures

Electrostriction-based scenario proposed by M. N. Shneider, M. Pekker and A. Fridman

Shneider, M. ; Pekker, M. ; Fridman, A. IEEE Transactions on Dielectrics and Electrical Insulation Vol. 19, No. 5; 2012

Seepersad et al. 2013 *J. Phys. D: Appl. Phys*. **46** 355201

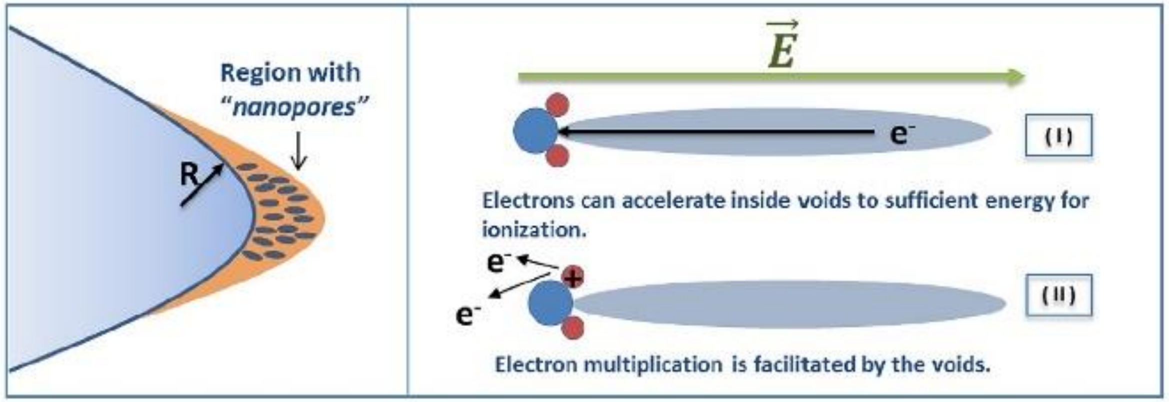

$$\vec{F} = \frac{\varepsilon_0}{2}\nabla\left(E^2 \frac{\partial\varepsilon}{\partial\rho}\rho\right) \approx \xi\varepsilon_0\varepsilon\nabla E^2 \quad (\xi \approx 1)$$

$$P_{\text{total}} = P_{\text{hydr}} - P_{\text{electr}} = P_{\text{hydr}} - \rho\varepsilon_0\left(\frac{\partial\varepsilon}{\partial\rho}\right)E^2$$

Computers and Mathematics with Applications 67 (2014) 340–349

Three-dimensional LBE simulations of a decay of liquid dielectrics with a solute gas into the system of gas–vapor channels under the action of strong electric fields☆

A.L. Kupershtokh*

Lavrentyev Institute of Hydrodynamics SB RAS, Novosibirsk, Russia

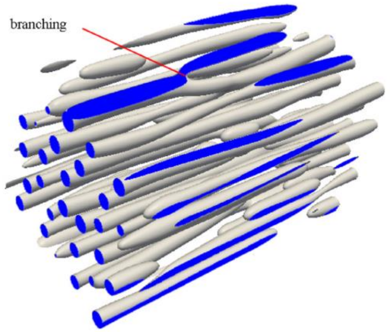

Fig. 6. The decay of a binary mixture in the three-dimensional strong electric field. Only the gas–vapor channels are shown. $\tilde{T} = 0.9$, $\tilde{\rho}_0 = 1.66$, $\tilde{A} = 60$, $B = -0.02$, $q = 0.02$, $\tau = 1$, $t = 1800$. The lattice is $192 \times 192 \times 352$.

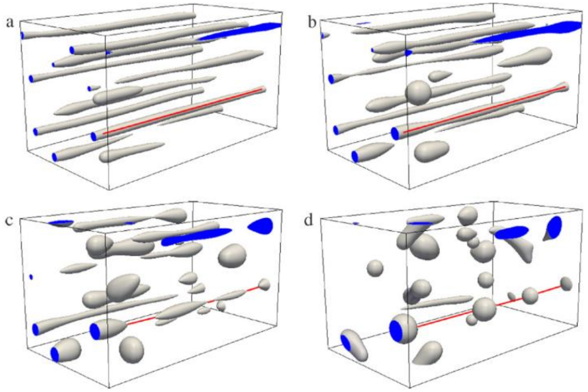

Fig. 8. The decay of the gas–vapor channels after turning off the electric field. Only the gas–vapor channels are shown. $\tilde{T} = 0.9$, $\tilde{\rho}_0 = 1.66$, $\tilde{A} = 30$, $B = -0.02$, $q = 0.02$, $\tau = 1$. The lattice is $192 \times 192 \times 352$. $t = 5600$ (a); 6600 (b); 7600 (c); 9000 (d).

Reactor needle-to-chamber wall geometry, the discharge generated by nanosecond pulsed HV power supply (**FID** Technology GmbH).

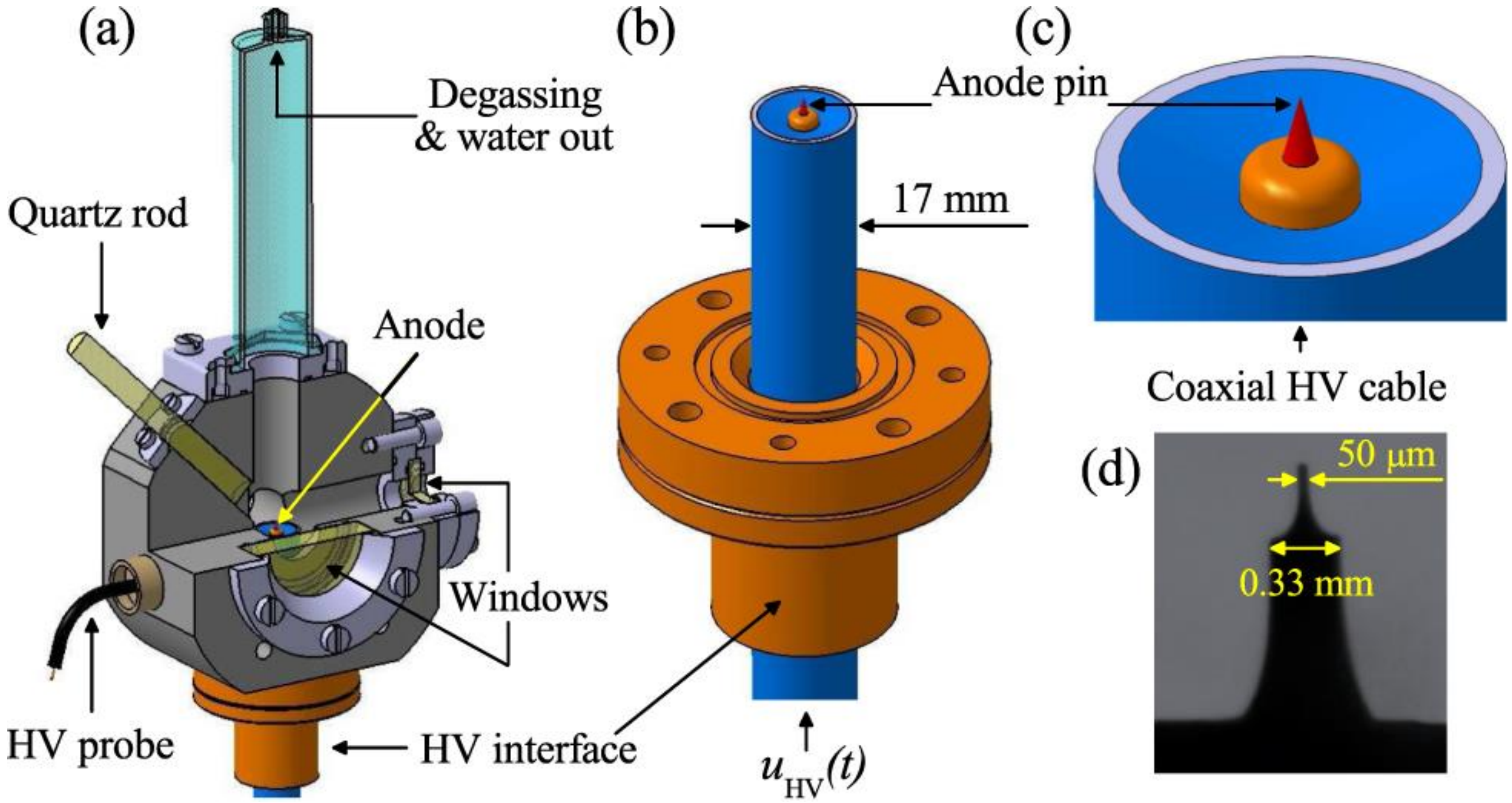

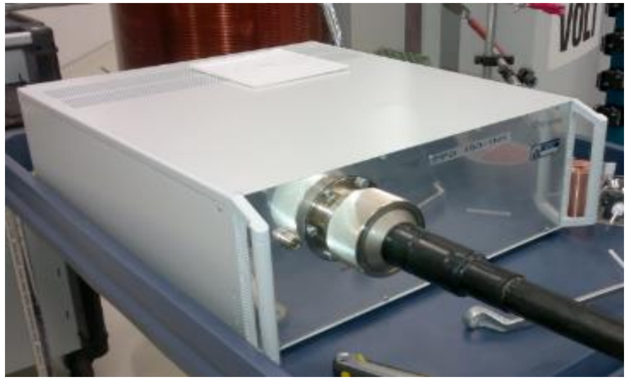

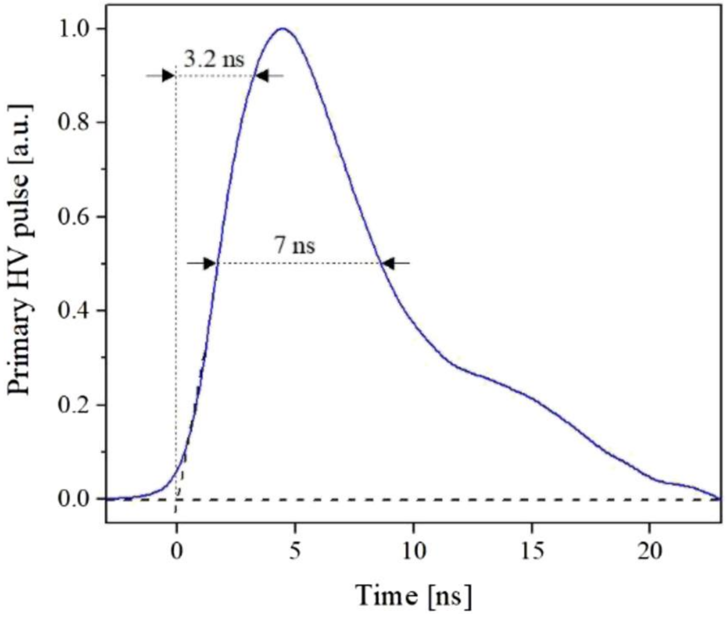

M Simek et al Plasma Sources Sci. Technol. 29 (2020) 064001

EXPERIMENT

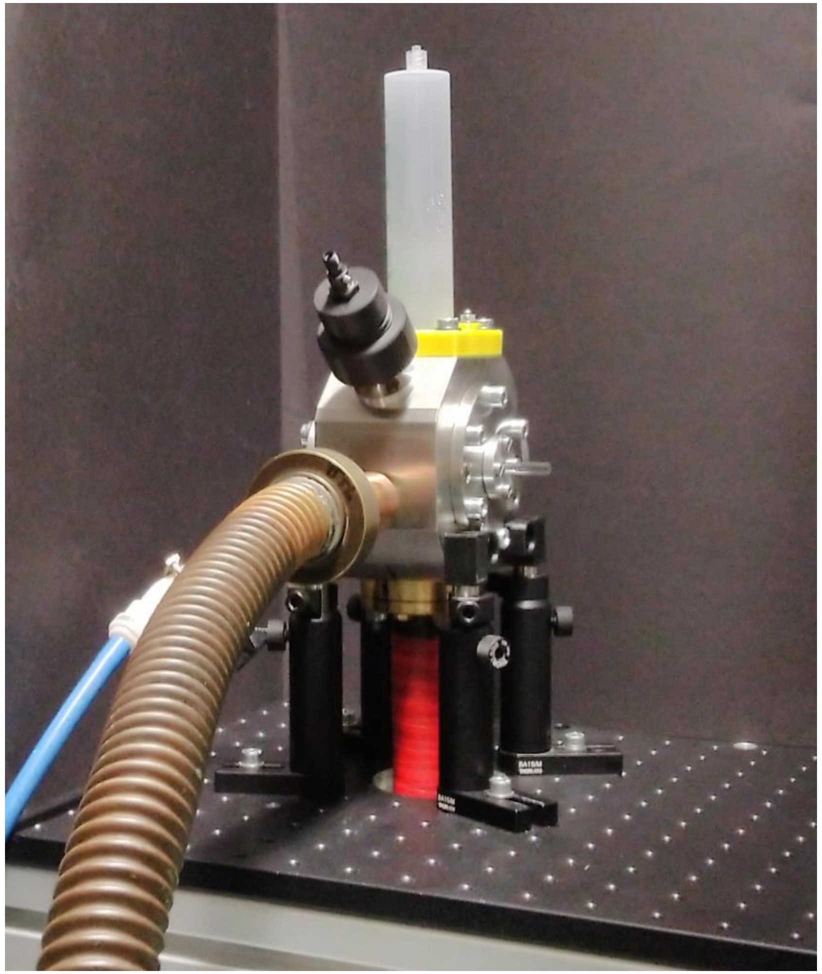

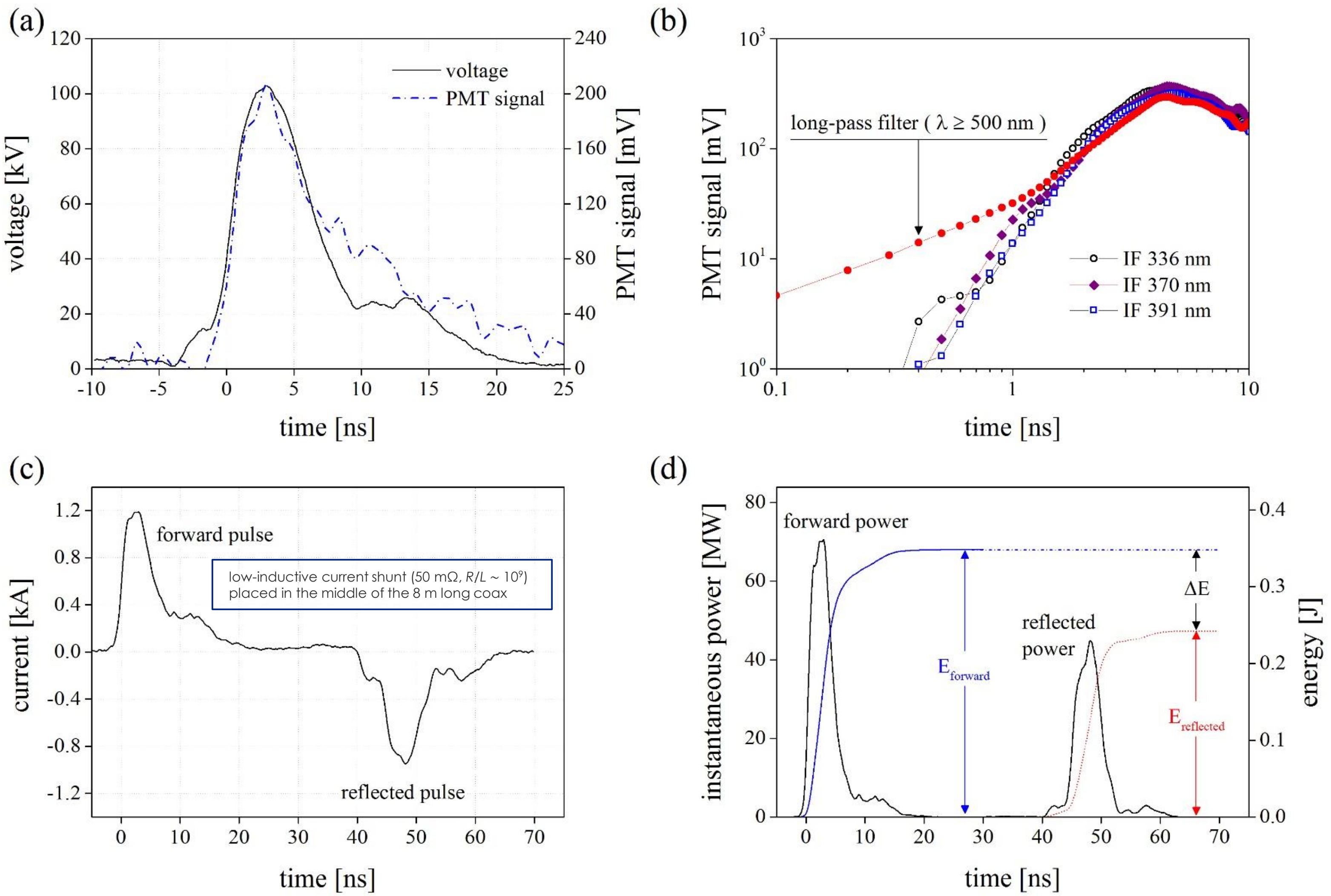

Milan Šimek et al 2017 Plasma Sources Sci. Technol. 26 07LT01

Single HV pulse - single HV burst - periodic HV

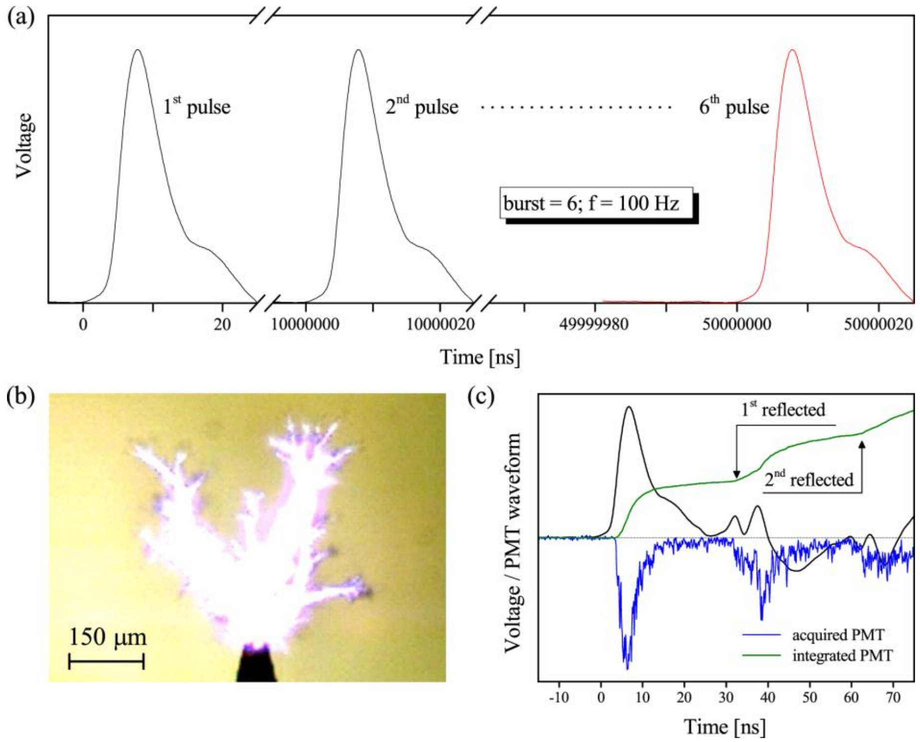

Sequence of six HV pulses (a) with the required amplitude is produced at a specific repetition frequency (*f* = 100 Hz). Each HV pulse causes a specific discharge event (b) composed of the primary discharge pulse followed with several discharges due to the reflected HV pulses visualized through the discharge-induced emission revealed by the PMT (c).

Petr Hoffer et al 2022 *Plasma Sources Sci. Technol.* 31 015005

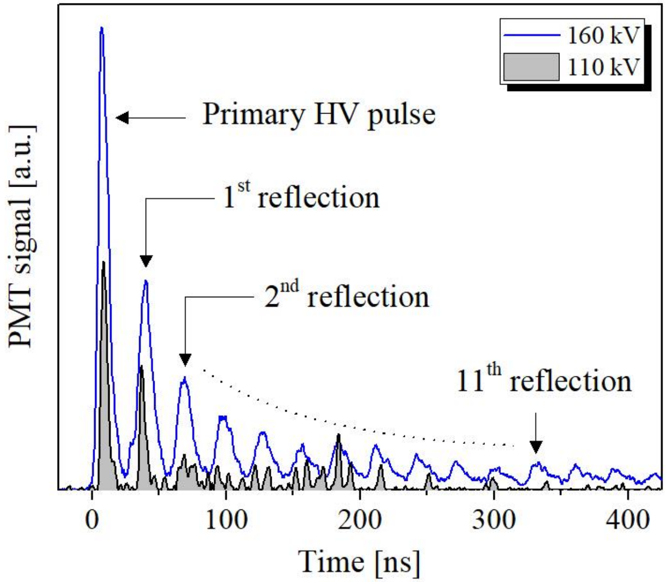

PIE waveforms characterizing pulsed HV discharge in DI water composed of the primary discharge event followed by a succession of gradually fading events caused by reflections of HV waveforms on the unmatched load. PIE registered by the ultrafast PMT and plotted for two different amplitudes of the primary HV pulse (anode side) of 110 kV and 160 kV.

M Simek et al Plasma Sources Sci. Technol. 29 (2020) 064001

Single HV pulse - single HV burst - periodic HV

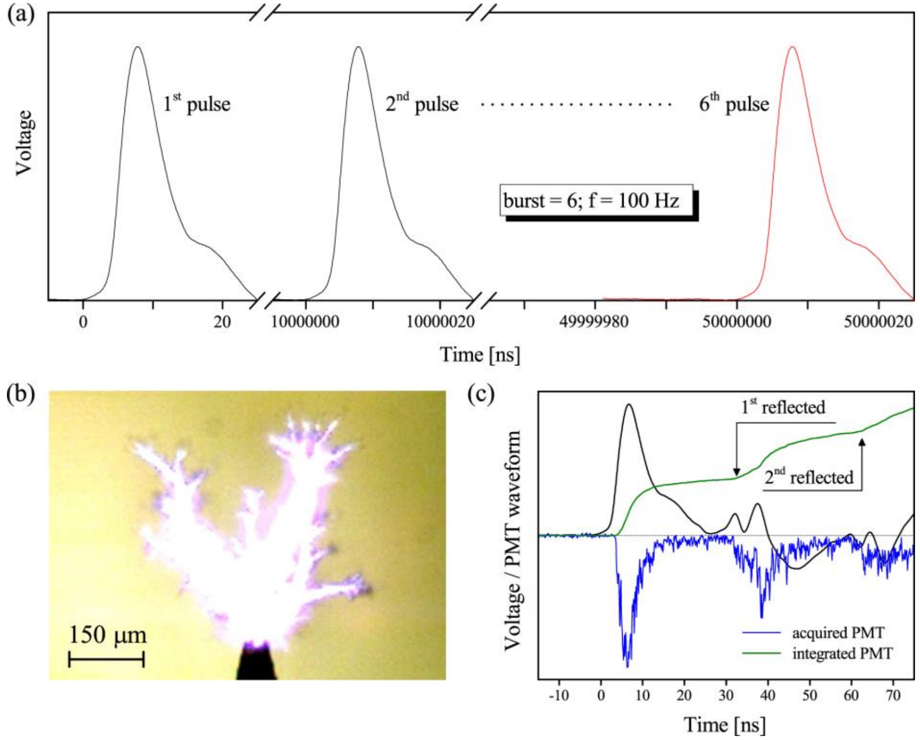

Sequence of six HV pulses (a) with the required amplitude is produced at a specific repetition frequency (*f* = 100 Hz). Each HV pulse causes a specific discharge event (b) composed of the primary discharge pulse followed with several discharges due to the reflected HV pulses visualized through the discharge-induced emission revealed by the PMT (c).

Petr Hoffer et al 2022 *Plasma Sources Sci. Technol.* 31 015005

Reproducibility issues

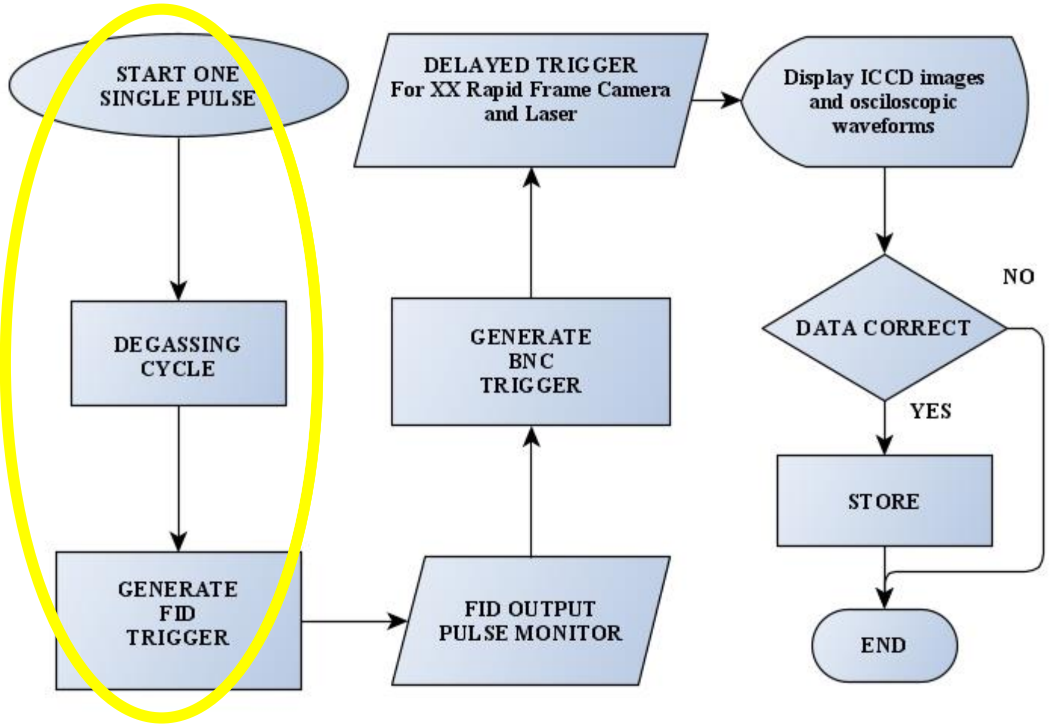

Flowchart of the LabVIEW VI program that controls the performance of a complete discharge cycle with subsequent data acquisition and storage.

Václav Prukner et al 2021 *Plasma* 4, no. 1: 183-200

ICCD (imaging) spectrometry:

JY iHR-320 + Andor iStar ICCD DH740 for UV-vis-NIR
(200 – 850 nm)

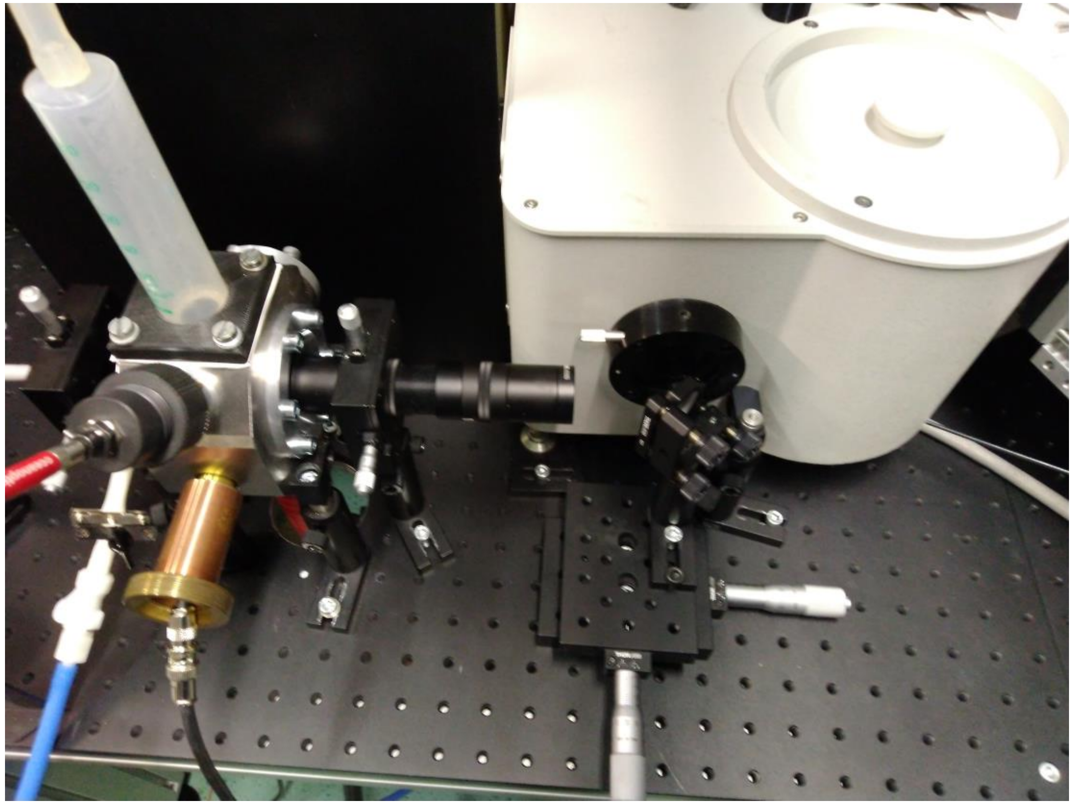

Andor Shamrock 303i +iStar ICCD DH340 for vis-NIR
(550 – 1100 nm)

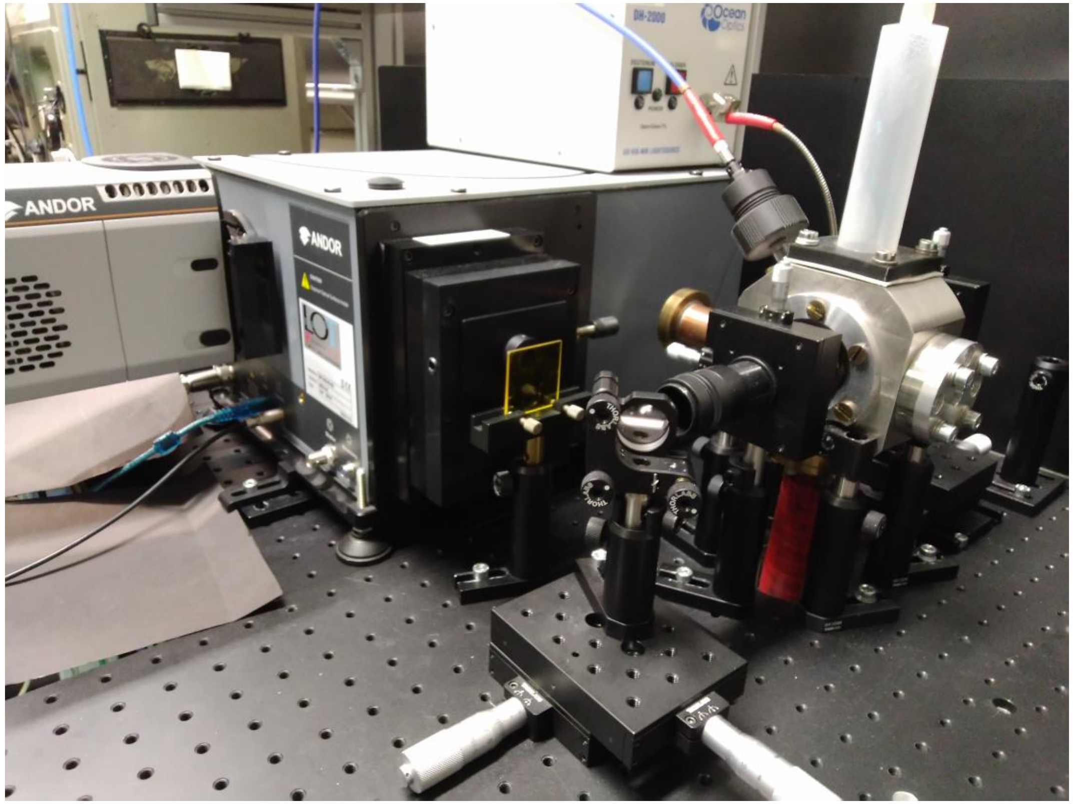

XXRapidFrame 4-channel framing camera (Stanford Computer Optics, Inc):

Four Channel ICCD System based on UV extended mirror image splitting optics and four 4-Picos/0.2ns, 200-820 nm

Combined with the Questar QM-1 long-distance microscope

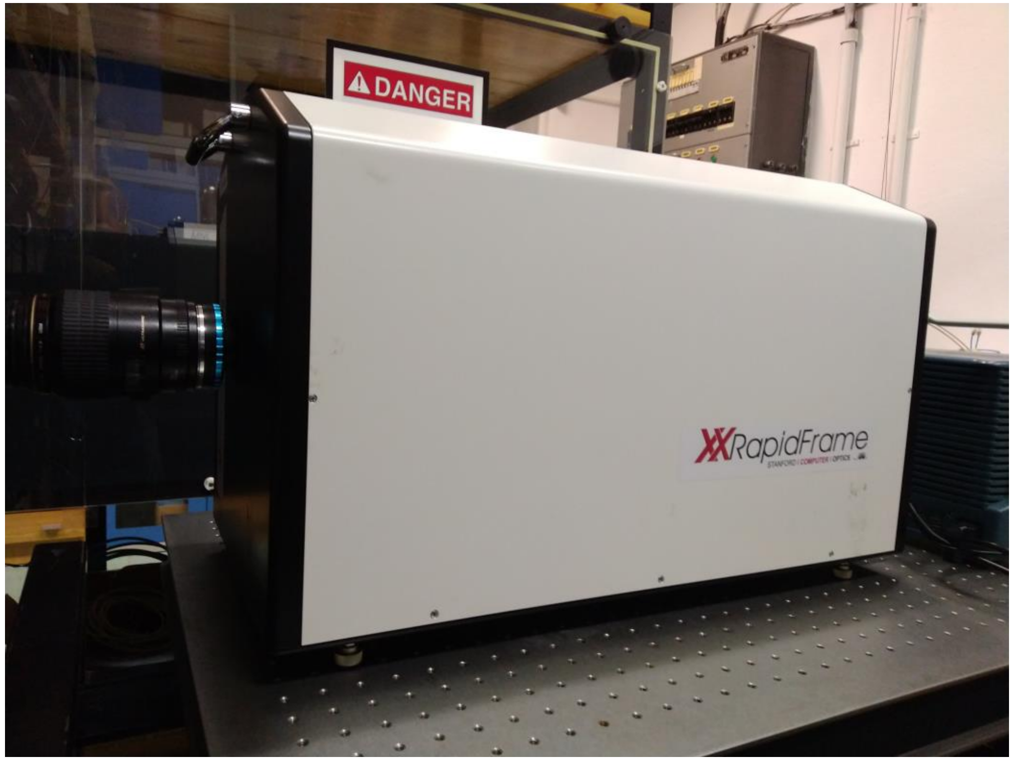

- Resolution **(256×152 px) => 4 microns/pixel**
- Minimum inter-frame delay of **7.7 microseconds** to record sequences of images in an infinite loop.
- Capturing events evolving in time-scales from **tens of microseconds to milliseconds and seconds.**

Phantom high-speed camera

v710

Ultra-fast – 1.4 million fps

1280 x 800 at 7500 fps

300 ns digital exposure

1. Picosecond shadowgraphy
2. Mach-Zehnder interferometry
3. Four synchronized ICCD detectors
4. High-speed framing camera
5. Optical emission spectroscopy

1. PICOSECOND SHADOWGRAPHY

- The laser light source was the Katana 05 (Onefive) system (with a **pulse duration of 35 ps** and up to 6 nJ at **532 nm**).
- Registration of shadowgraph images using a **CMOS camera (Canon 550D, 18 Mpx)** after appropriate magnification.
- BNC generator produced an input trigger for the Katana 05 laser with the required laser delay.

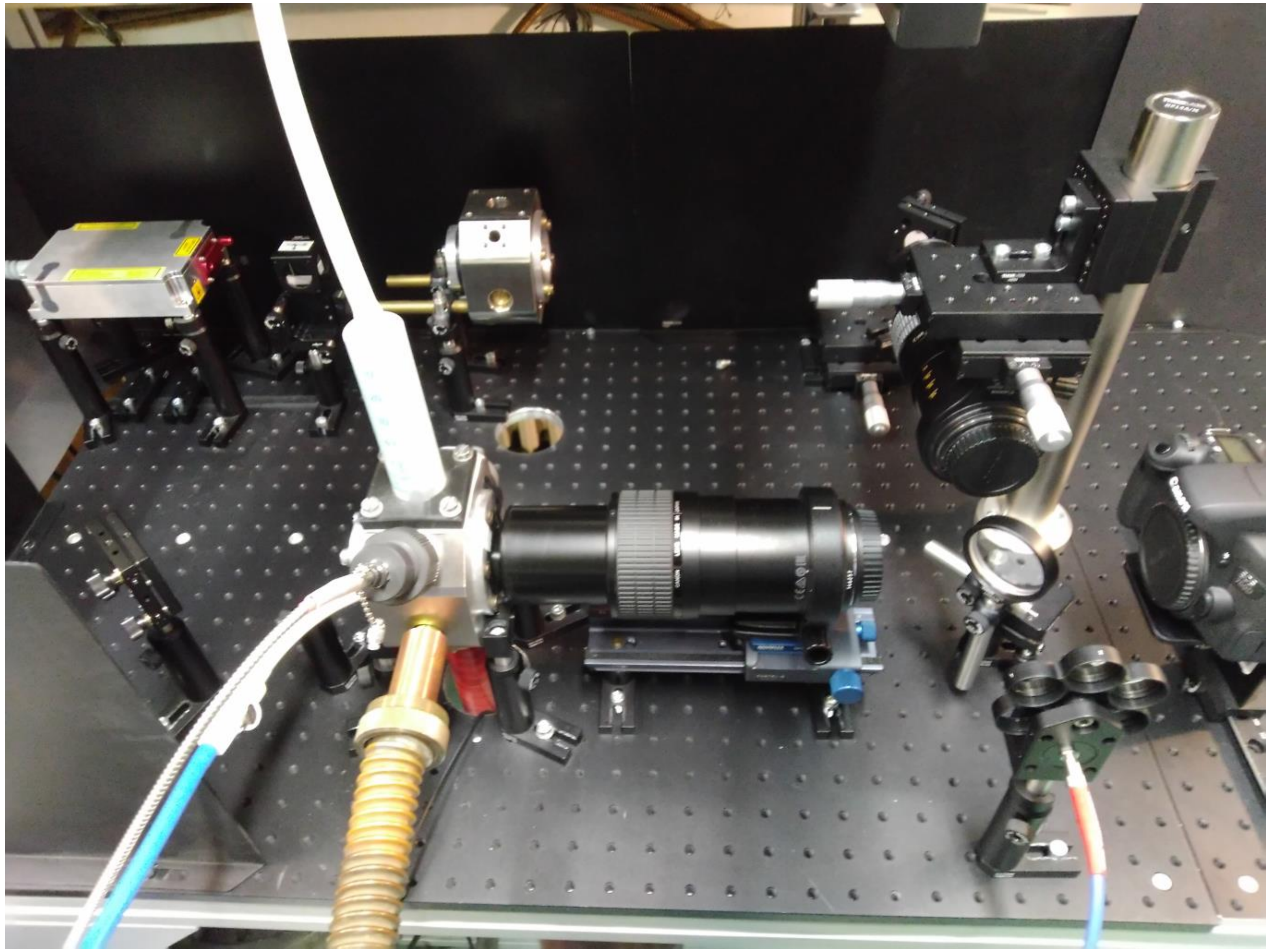

1. PICOSECOND SHADOWGRAPHY

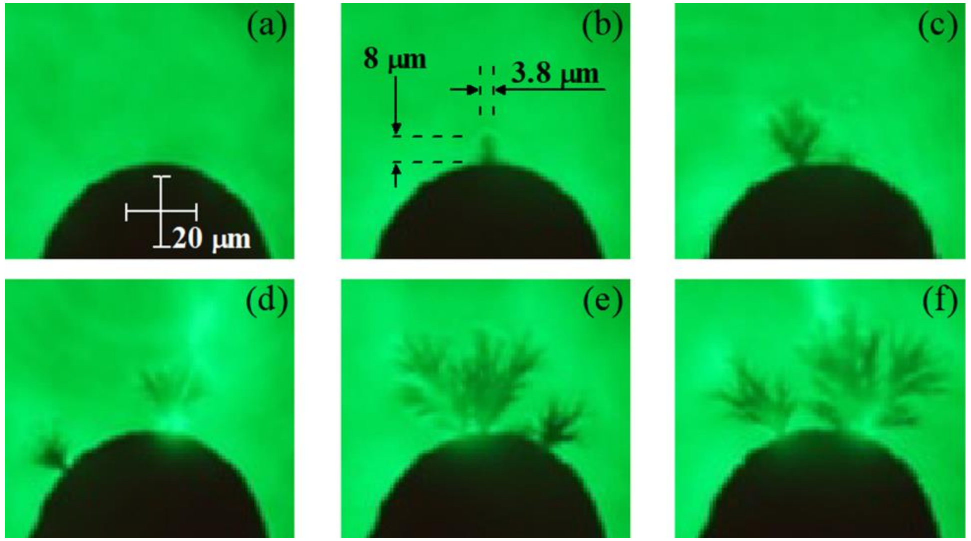

Sequence of shadowgraphic images captured with exposure of 1 s during the main HV pulse for various HV onset–laser pulse delays for a paraboloid-like anode stressed with HV pulse of 130 kV. Probing laser pulse delayed by (a) 2.8, (b) 3.3, (c) 3.5, (d) 3.6, (e) 3.7 and (f) 3.8 ns with respect to the HV pulse onset.

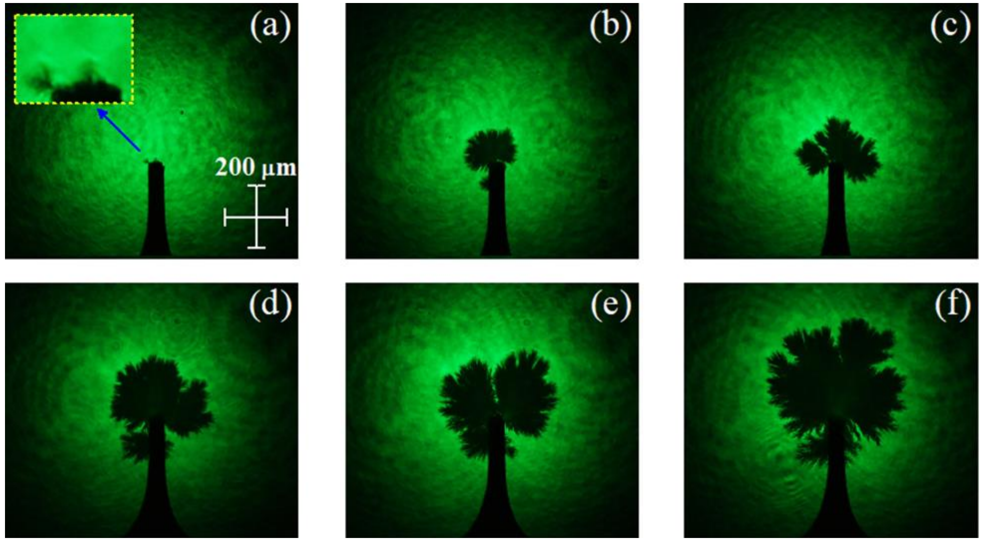

Sequence of shadowgraphic images captured during the main HV pulse for various HV onset–laser pulse delays for a hyperboloid-like anode stressed with HV pulse of 110 kV. Probing laser pulse delayed by (a) 2.4, (b) 3.1, (c) 3.5, (d) 4.1, (e) 4.2 and (f) 5.1 ns with respect to the HV pulse onset.

M Simek et al Plasma Sources Sci. Technol. 29 (2020) 064001

1. PICOSECOND SHADOWGRAPHY

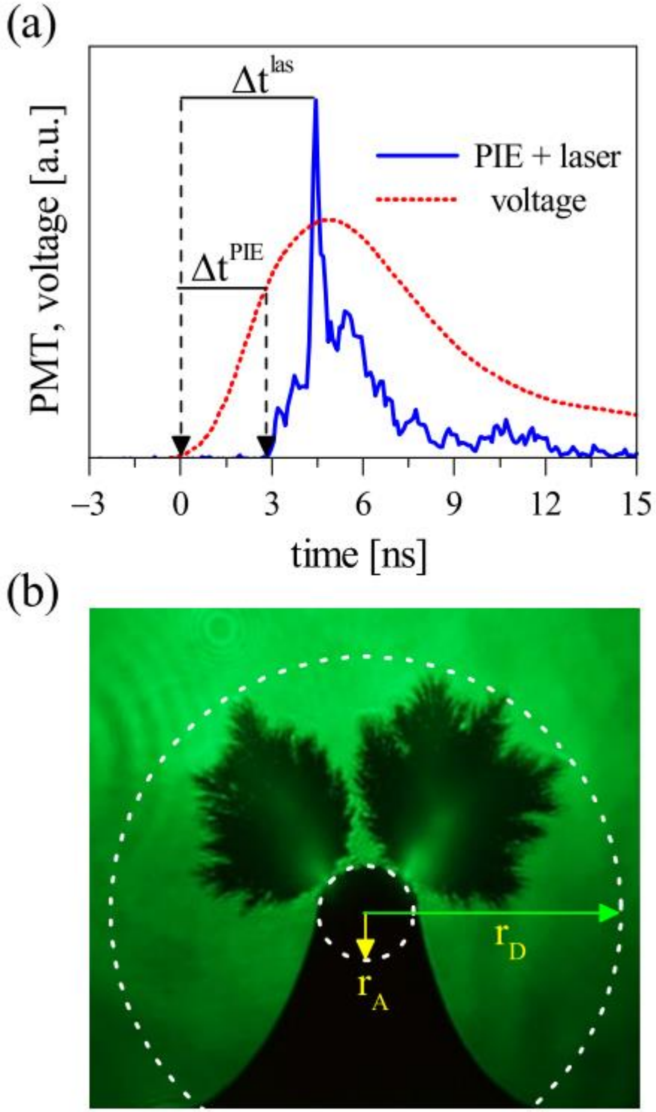

Basic opto-electrical discharge characteristics and lengths of the dark discharge filaments evaluated from associated shadowgraph images. The (a1)–(a3) and (b1)–(b3) panels show the data obtained for the paraboloid and hyperboloid-like anodes, respectively.

The (a1)/(b1)and (a2)/(b2) track anode HV and PIE waveforms for respective anode shapes (shown in inset). The (a3)/(b3) capture the evolution of the lengths of dark discharge filaments associated with a given delay of the laser pulse.

The formation time of the first (dark) phase is approximately 3–4 nanoseconds (after the onset of anode HV).

It takes approximately 600–800 ps after observing the first dark filaments to reveal the first PIE signal by the PMT.

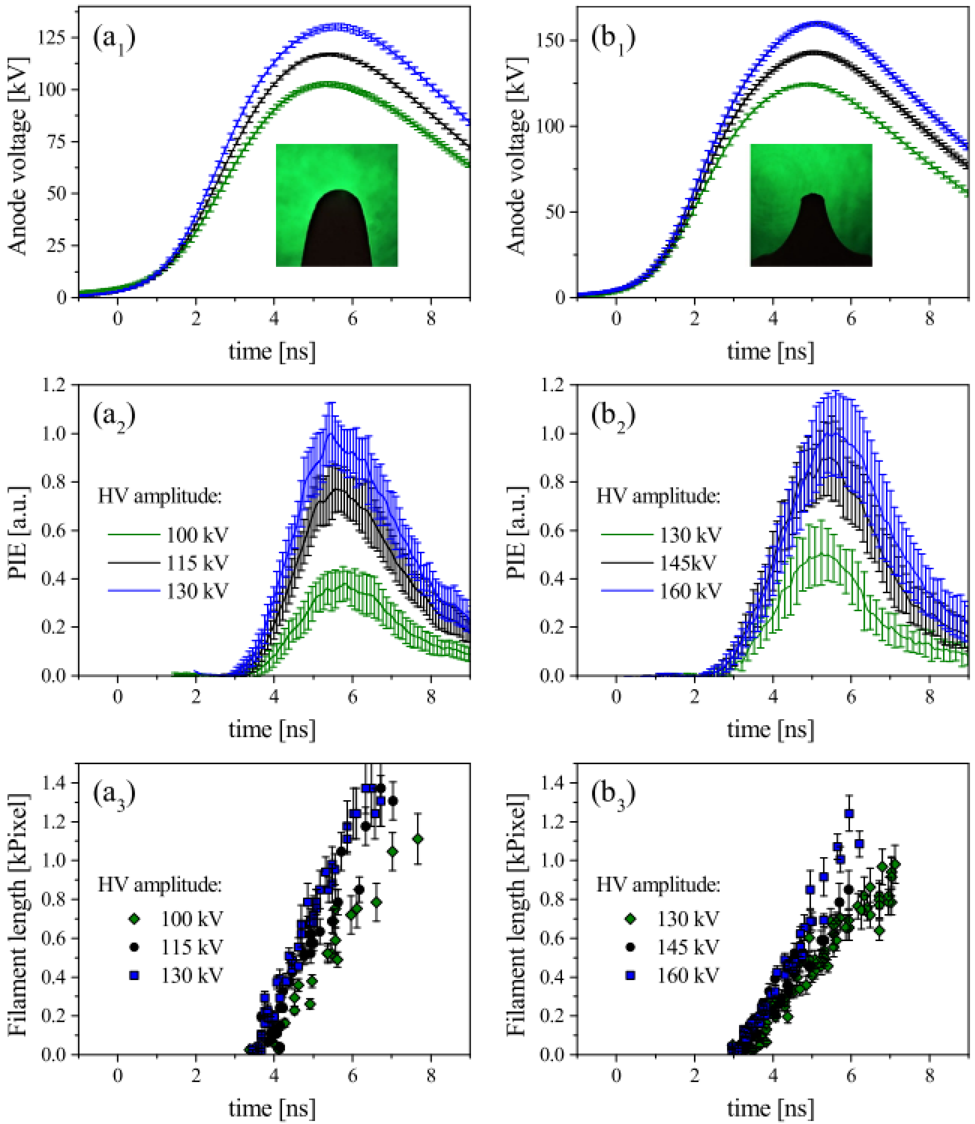

M Simek et al *Plasma Sources Sci. Technol.* 29 (2020) 095001

1. PICOSECOND SHADOWGRAPHY

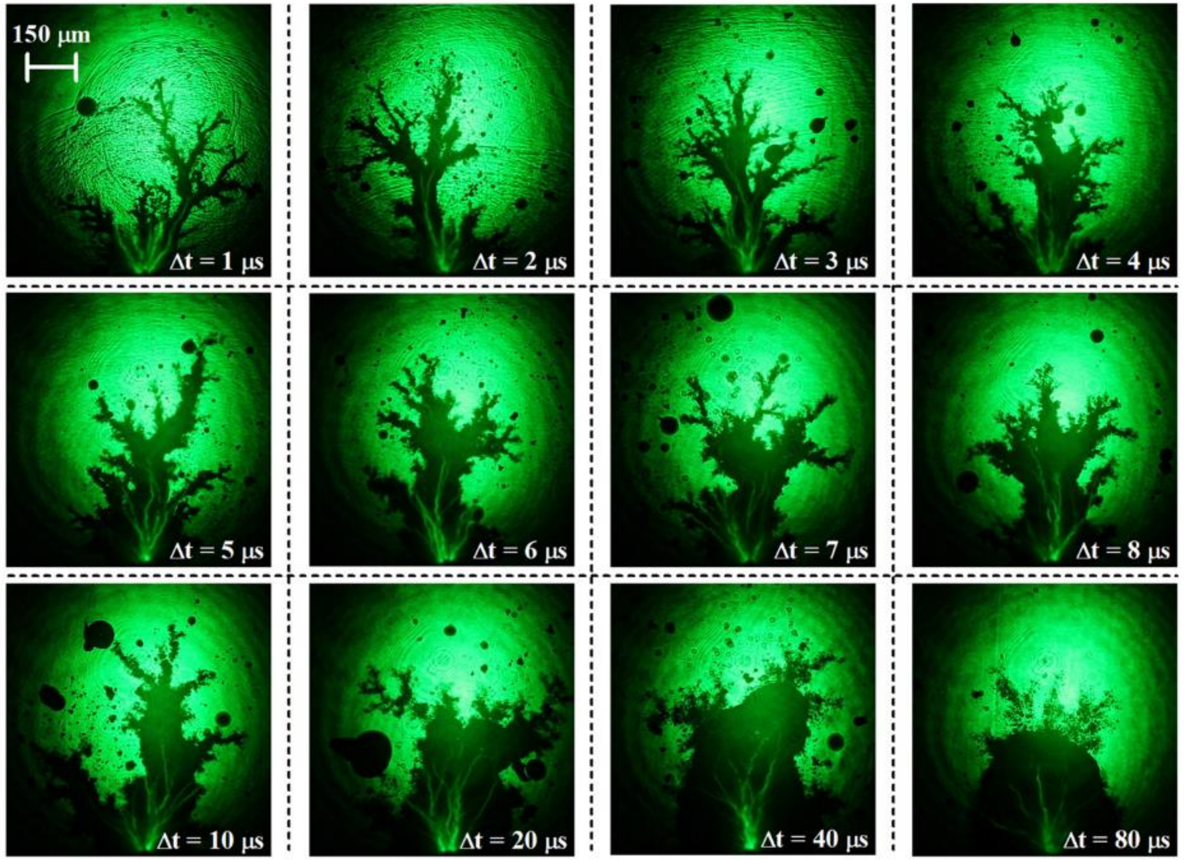

Figure 9. Selected shadowgraph images revealing the process of formation of gaseous structures from the discharge filaments in microsecond timescales (Δt indicates delay after the onset of the 6[th] HV pulse in the burst). Images acquired at a fixed repetition frequency ($f = 15$ Hz) and HV amplitude (145 kV on the anode side) of applied HV pulses.

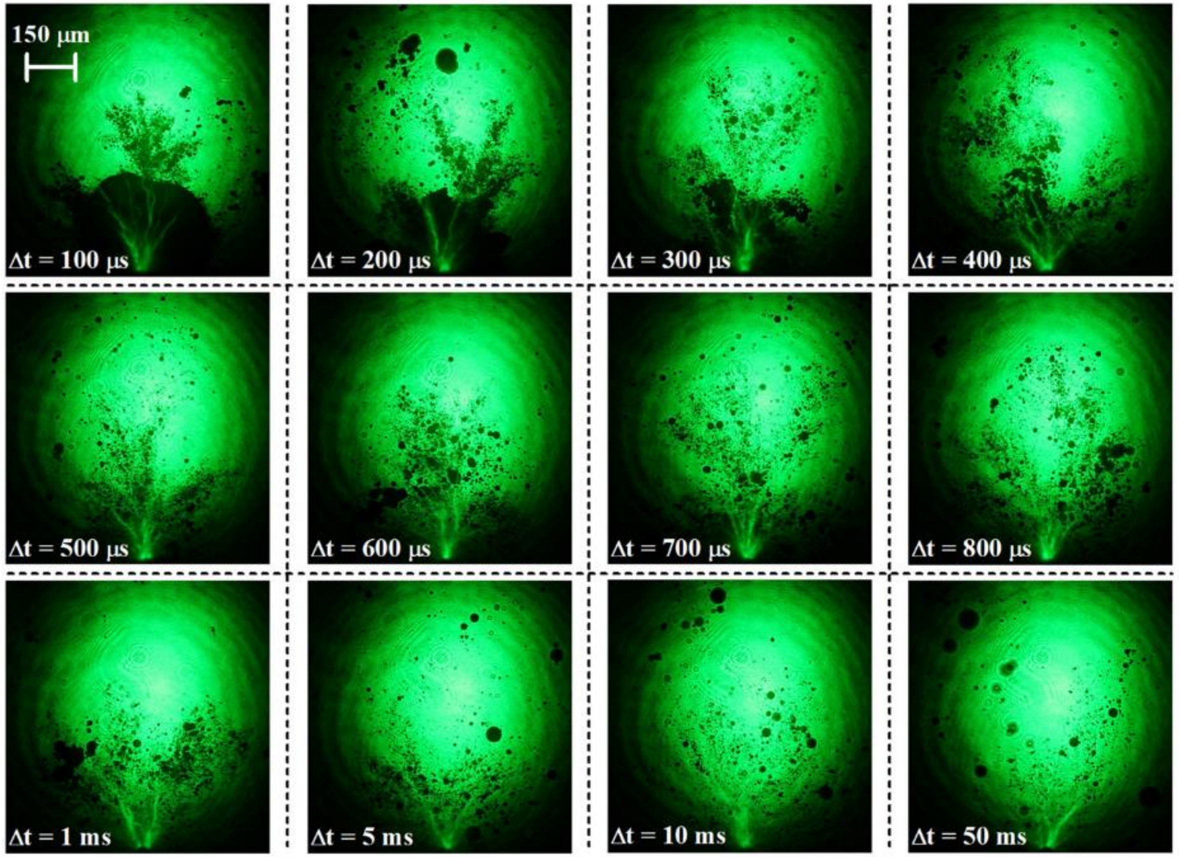

Figure 10. Selected shadowgraph images revealing the process of dissipation of gaseous structures in millisecond timescales previously formed in microsecond timescales from the discharge filaments (Δt indicates the delay after the onset of the 6[th] HV pulse in the burst). Images acquired at a fixed repetition frequency ($f = 15$ Hz) and an HV amplitude (145 kV on the anode side) of applied HV pulses.

Petr Hoffer et al 2022 *Plasma Sources Sci. Technol.* 31 015005

Microbubbles (non-condensable gases, H2 / O2) evidently perturb the anode area, and therefore the initial phase of the discharge

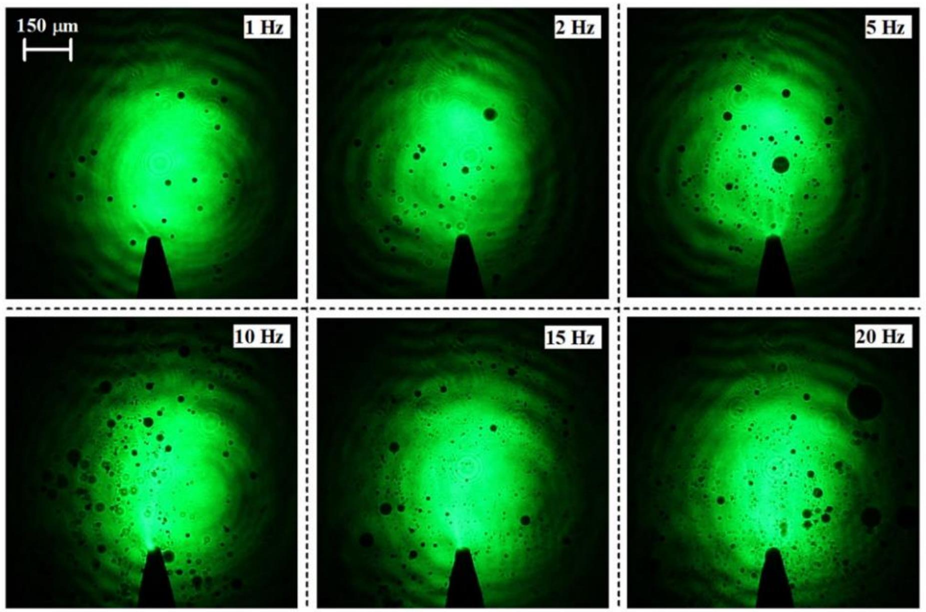

Figure 7. Selected shadowgraph images capturing the instantaneous distribution of microbubbles in the anode region just before the onset of the 6th HV pulse in the burst. Initial discharge conditions captured at various repetition frequencies ($f = 1$–20 Hz) at a fixed amplitude of applied HV pulses (145 kV on the anode side).

Burst mode: Serves as a good approximation of the periodic mode at higher frequencies up to 100 Hz (limited anode heating and erosion)

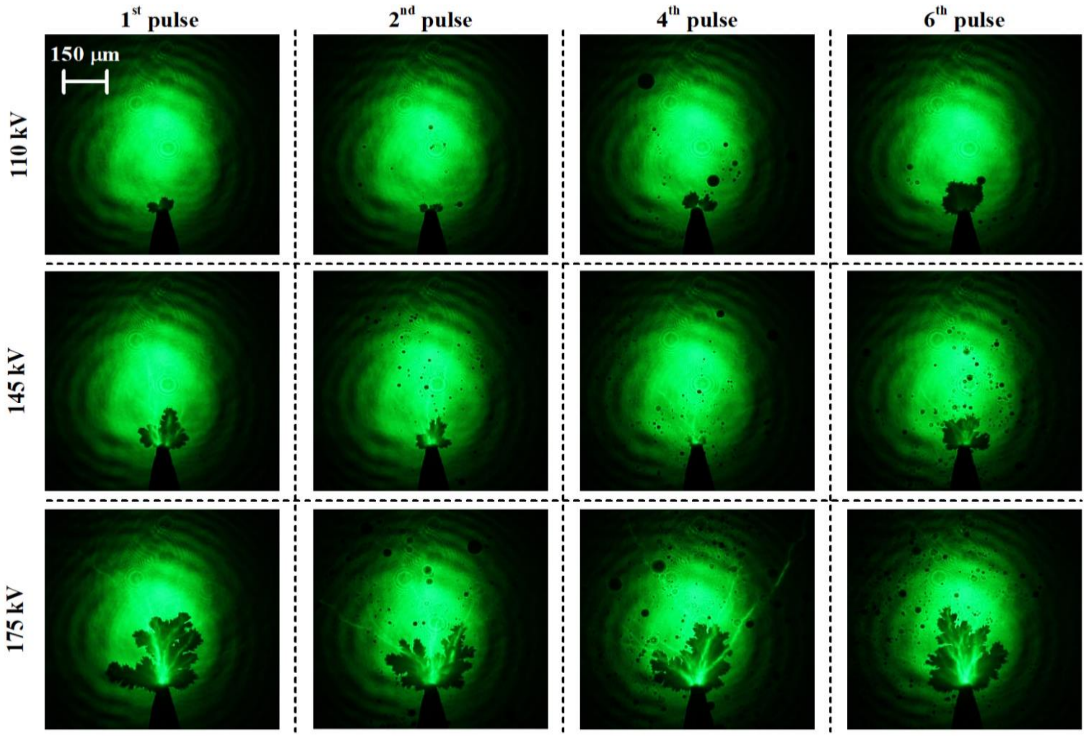

Figure 6. Selected shadowgraph images capturing instantaneous distribution of microbubbles in the anode region just after the onset of the dark discharge phase. The discharge is initiated by the n^{th} pulse in the HV burst ($f = 5$ Hz) at various amplitudes of the applied HV pulses (110/145/175 kV on the anode side).

Petr Hoffer et al 2022 *Plasma Sources Sci. Technol.* 31 015005

1. PICOSECOND SHADOWGRAPHY

In the case of gaseous micro-bubbles present in the anode region, the discharge filaments interfere with the bubbles located along their trajectory

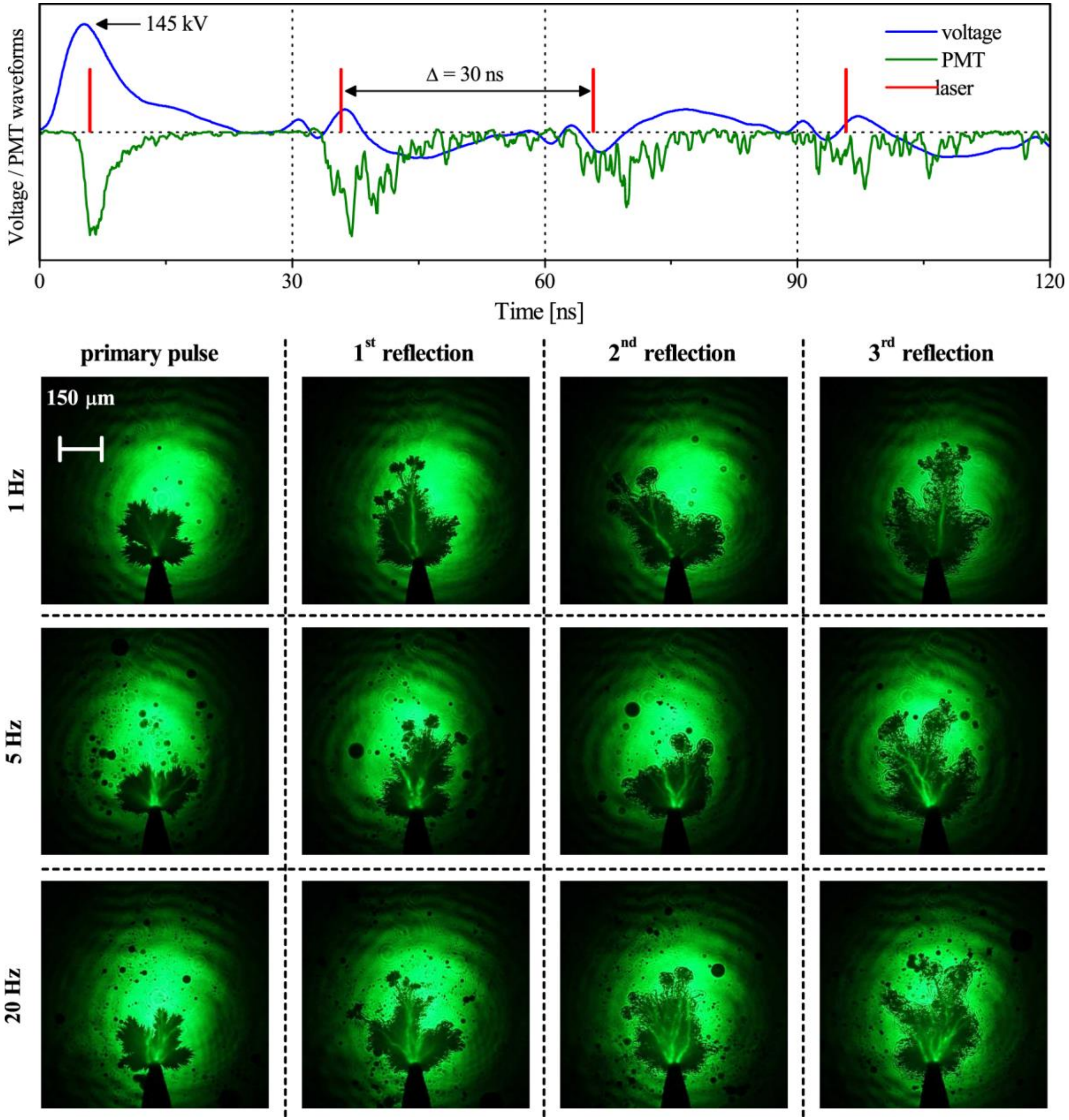

Selected shadowgraph images revealing the instantaneous distribution of microbubbles together with the extension of the dark discharge phase. Position of the probing laser with respect to the voltage/MPT waveforms is schematically shown in (upper waveforms); images captured during the 6th HV pulse in the burst are shown in (bottom images). The first column displays images taken during the primary HV pulse, while the other three columns characterize the first three HV reflections at various repetition frequencies (*f* = 1/5/20 Hz) and at fixed amplitude of applied HV pulses (145 kV on the anode side).

Petr Hoffer et al 2022 *Plasma Sources Sci. Technol.* 31 015005

2. MACH-ZEHNDER INTERFEROMETRY

- Nd:YAG laser (532 nm, 30 ps)
- **Shifts of the fringes** in interference patterns due to **variations in the refractive index**.
- Utilising a well-known **relation between the refractive index and pressure** in bulk liquid water.
- **Picosecond (30 ps)** resolutions in time and **micrometre (0.8 microns)** resolutions in space.

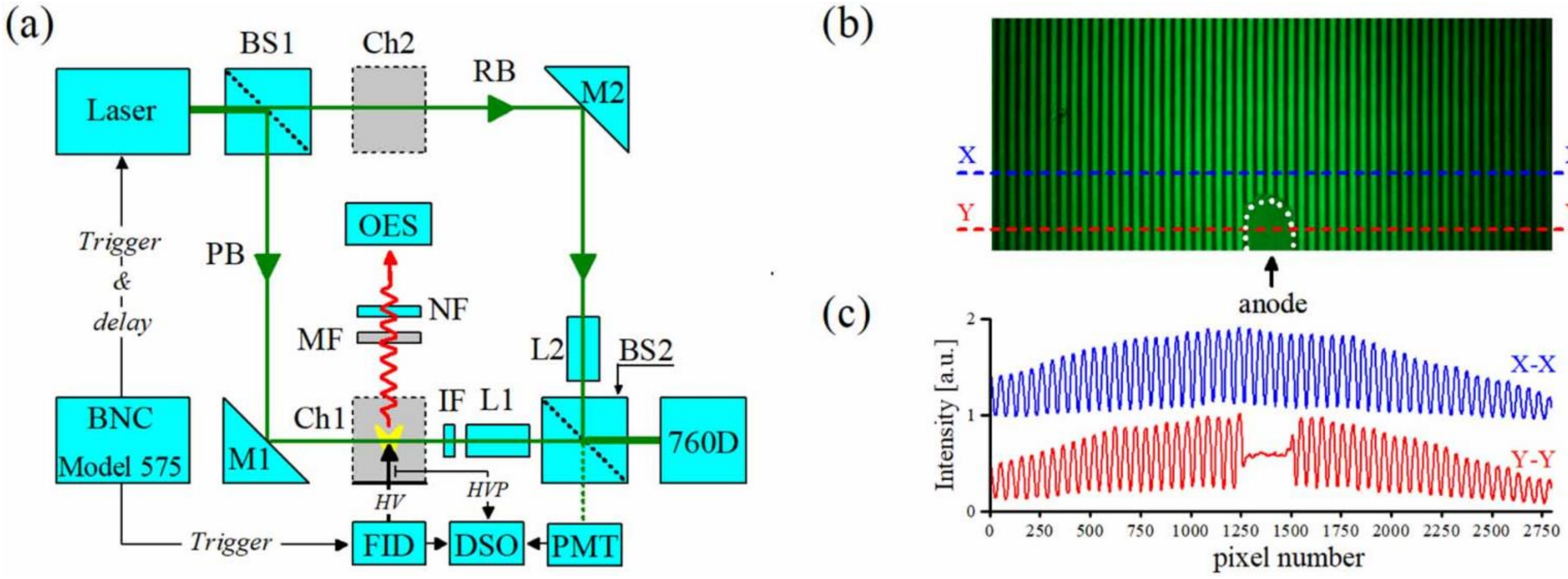

Petr Hoffer et al 2021 J. Phys. D: Appl. Phys. 54 285202

2. MACH-ZEHNDER INTERFEROMETRY

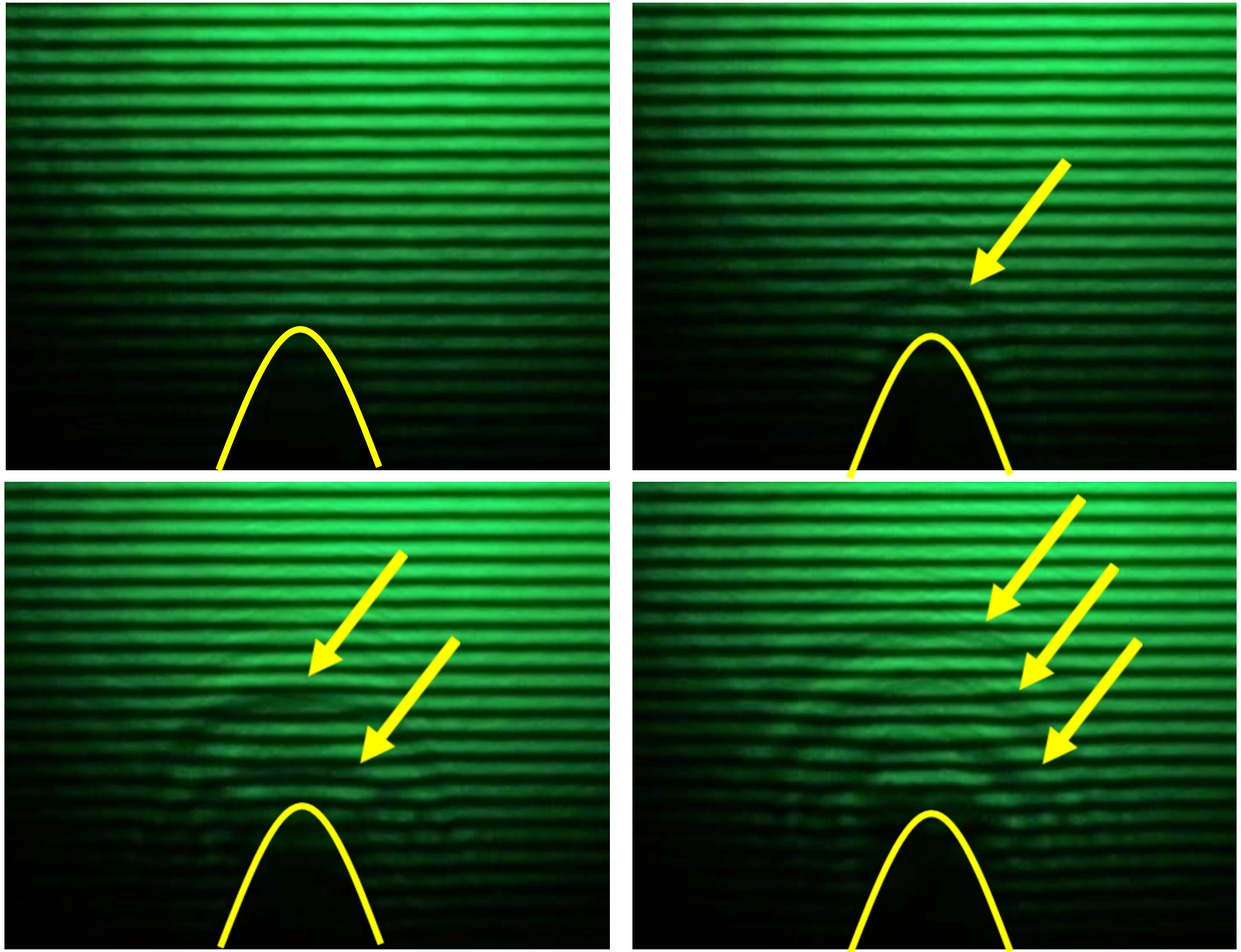

Interferometric images of subcritical non-discharge events

Interferometric images characterizing two distinct discharge morphologies occurring in non-degassed DI water under single nanosecond HV pulse conditions

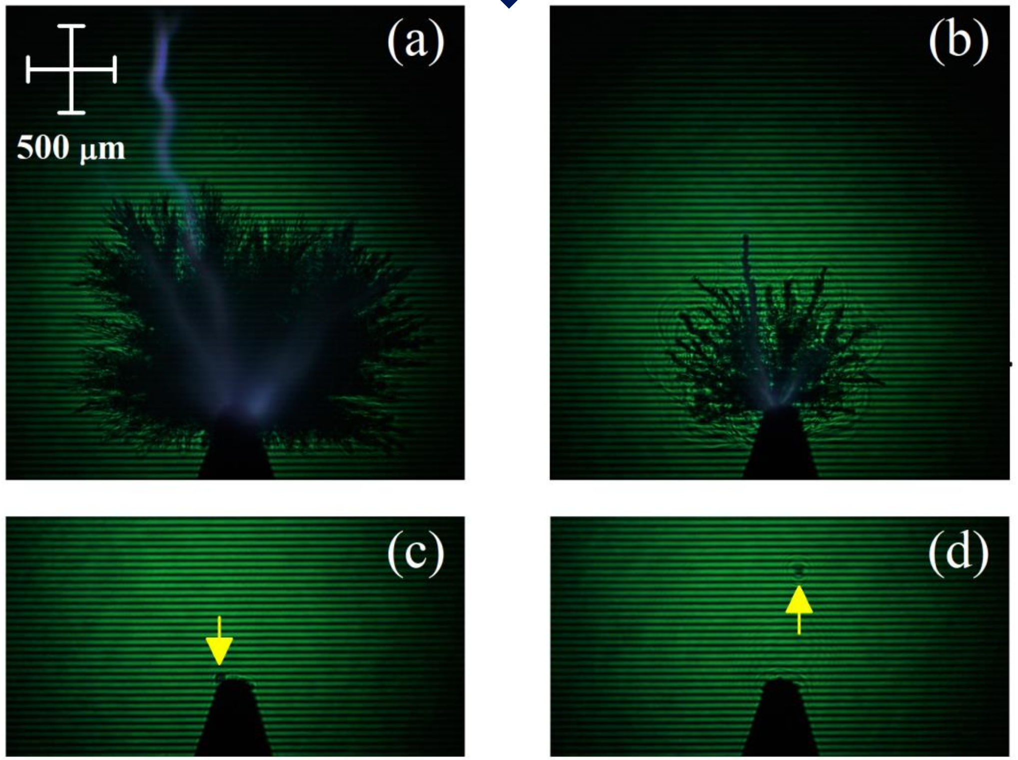

M Simek et al *Plasma Sources Sci. Technol.* 29 (2020) 095001

Sequence of ps interferometric images of single discharge events:

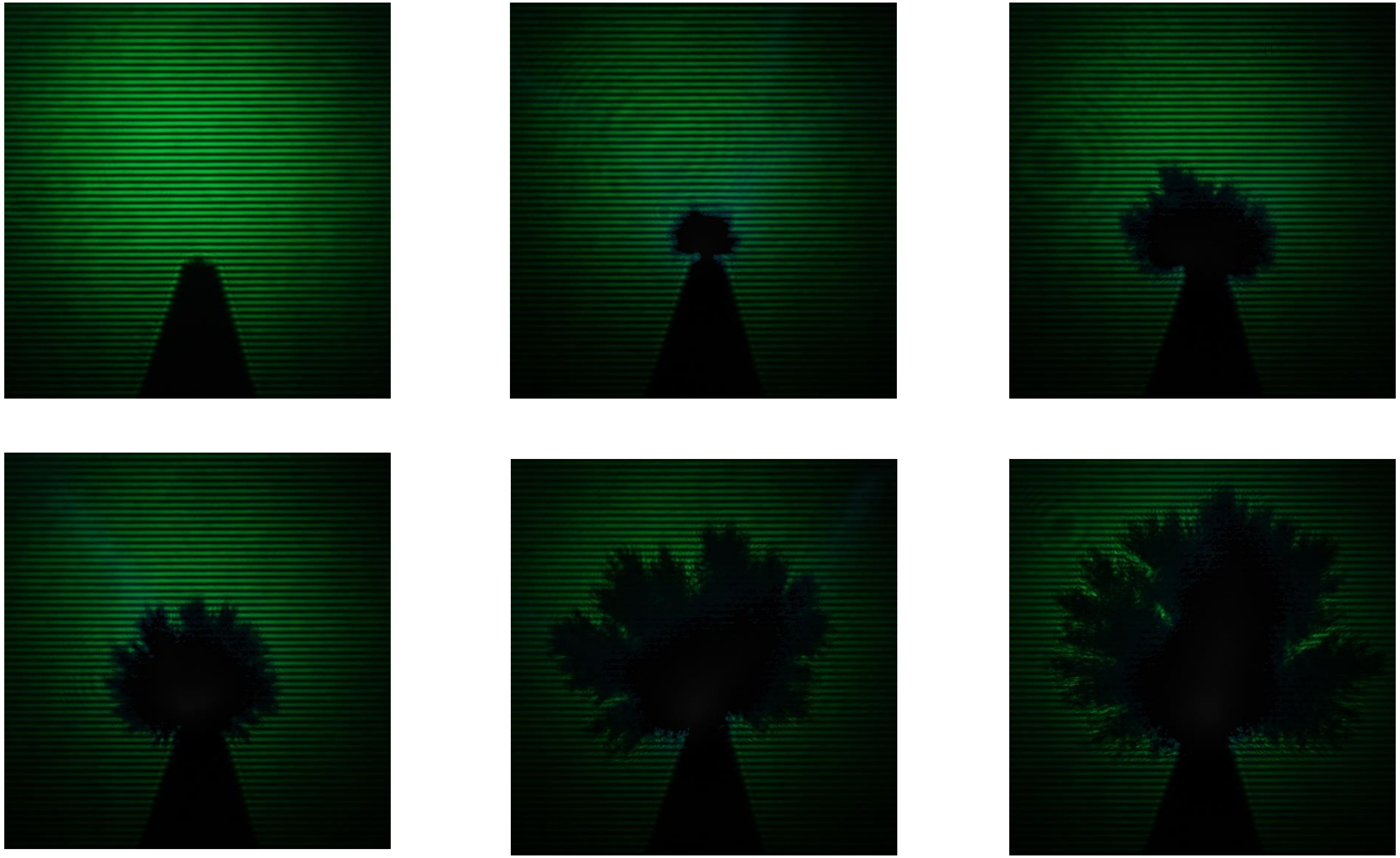

M Simek et al *Plasma Sources Sci. Technol.* 29 (2020) 095001

2. MACH-ZEHNDER INTERFEROMETRY

Petr Hoffer et al 2021 J. Phys. D: Appl. Phys. 54 285202

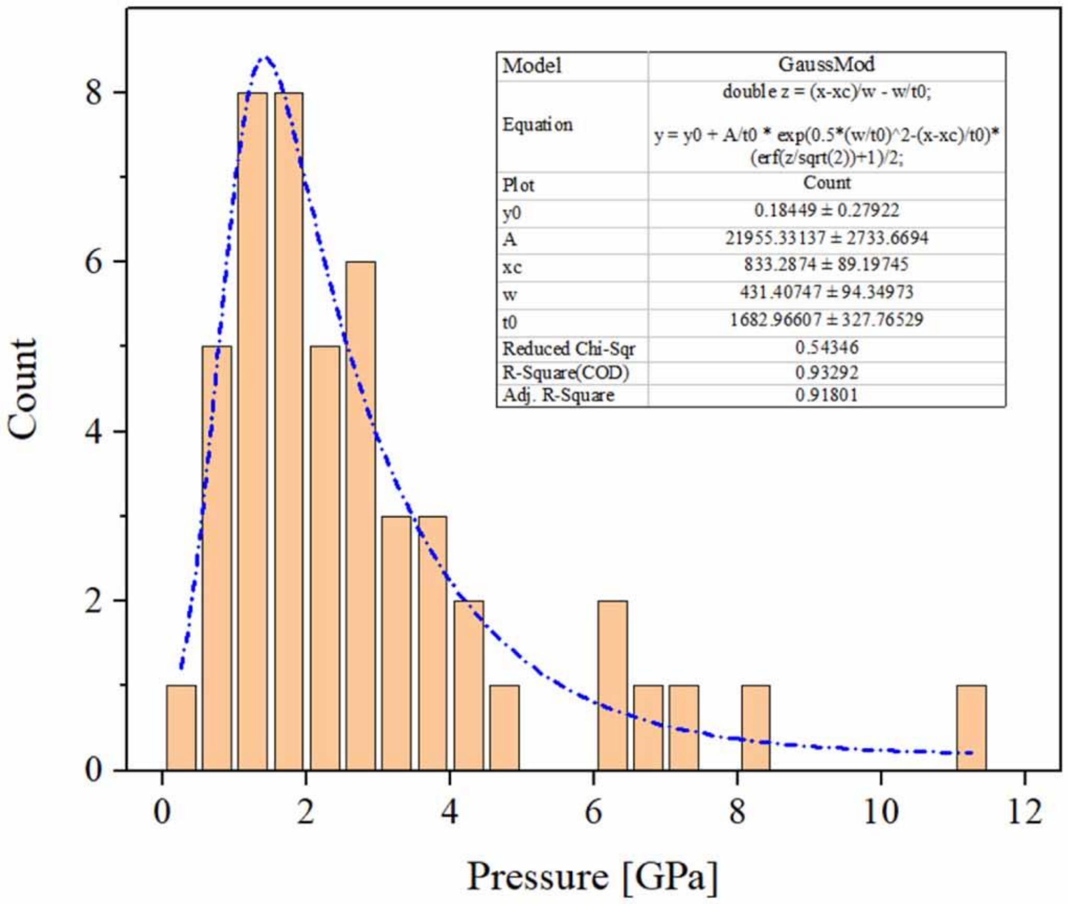

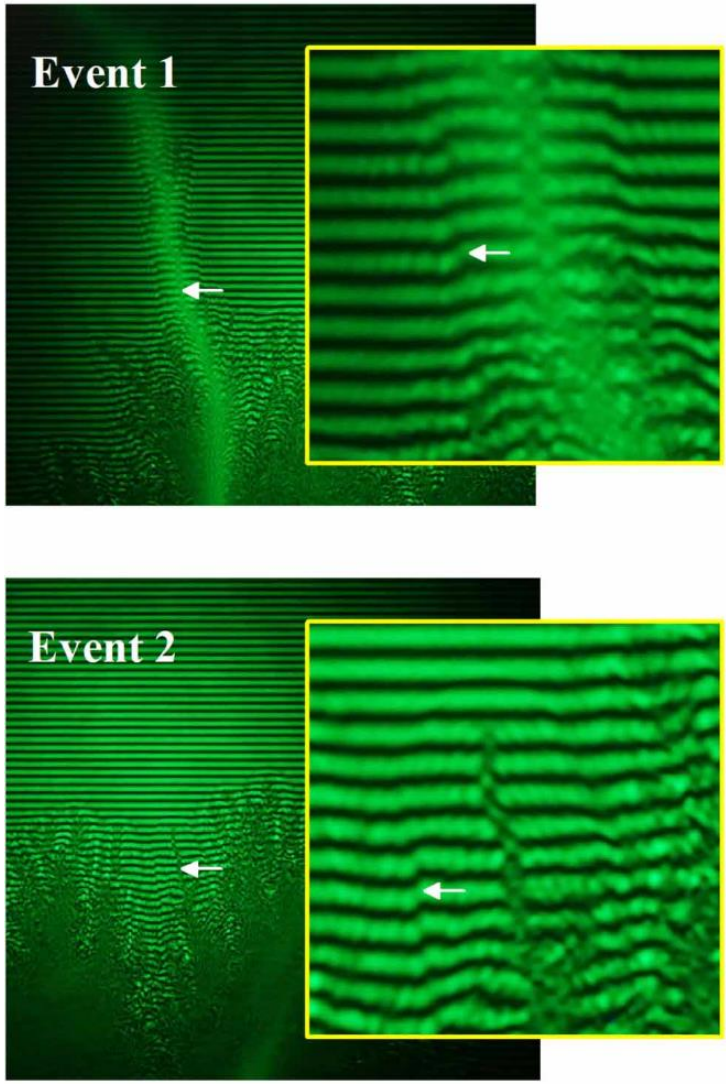

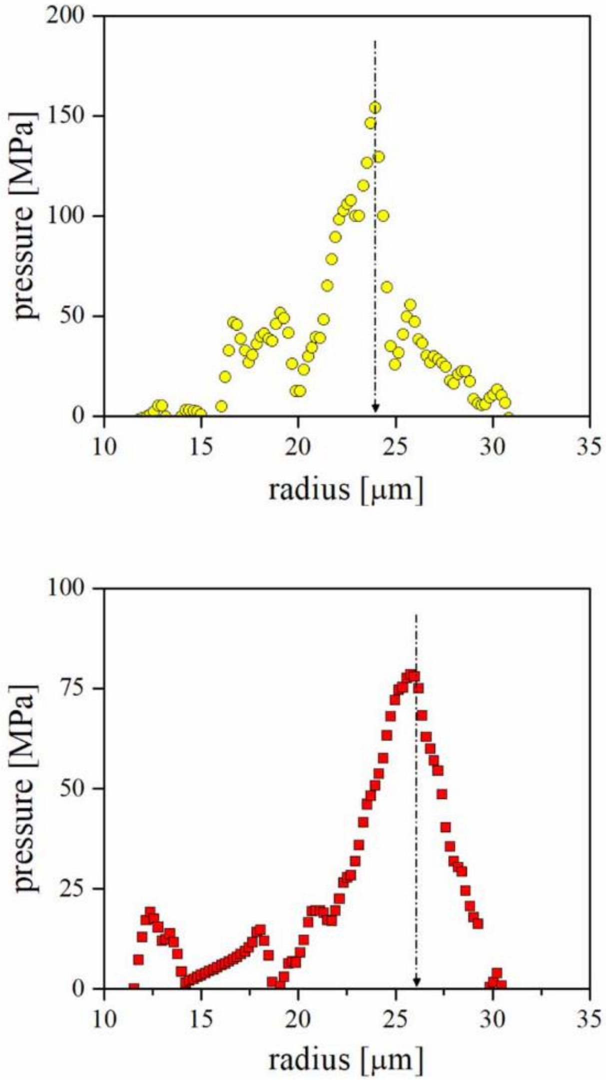

Most of those extraordinary strong shock-fronts were associated with the dark filaments containing strong residual plasma-induced emission.

3. FOUR SYNCHRONIZED ICCD DETECTORS

We combine a long-distance microscope with a four-channel image splitter fitted with four synchronised intensified charge-coupled device (ICCD) detectors, registering four magnified images per event.

- Temporal resolution down to **500 ps** and a spatial resolution of **3.6 µm/pixel**.
- The resolution of each 4-Picos ICCD detector is **780 × 580 pixels** with a bit depth of **12 bits.**

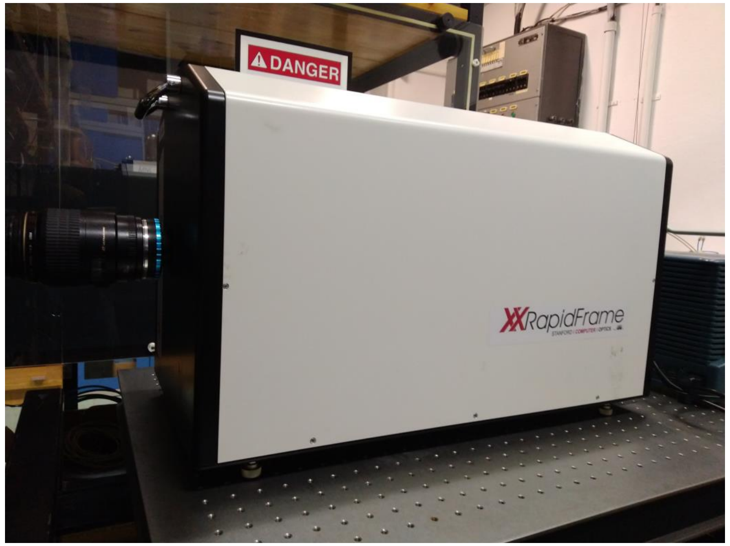

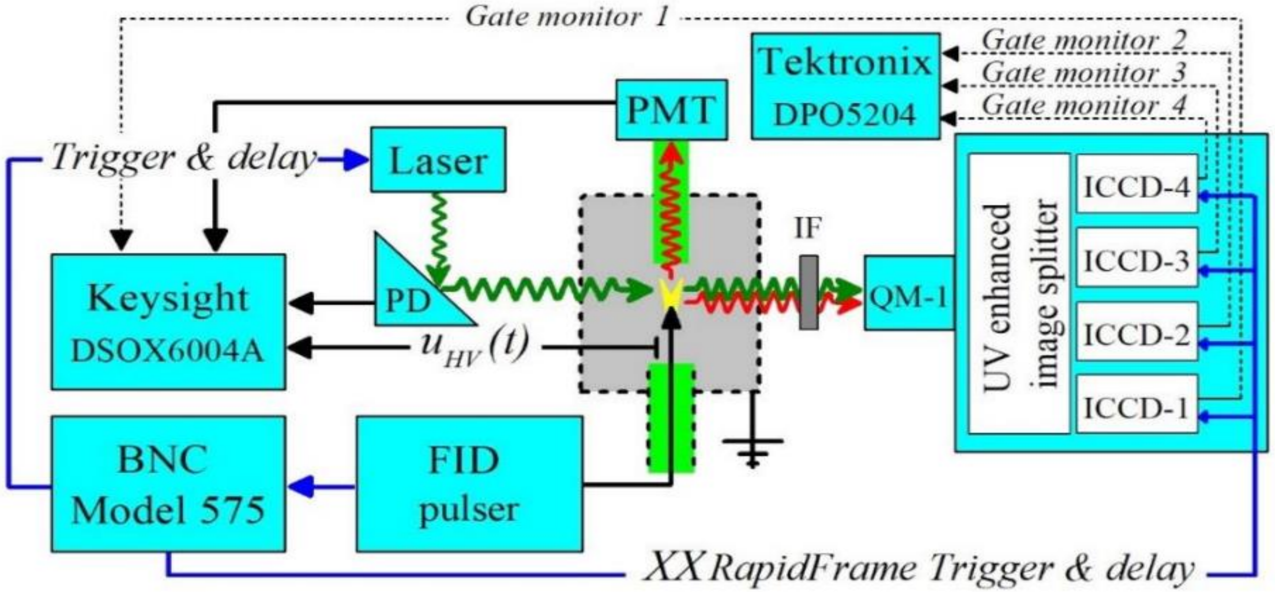

Prukner, V.; Schmidt, J.; Hoffer, P.; Šimek, M. Demonstration of Dynamics of Nanosecond Discharge in Liquid Water Using Four-Channel Time-Resolved ICCD Microscopy. Plasma 2021, 4, 183-200.

We combine a long-distance microscope with a four-channel image splitter fitted with four synchronised intensified charge-coupled device (ICCD) detectors, registering four magnified images per event.

- Temporal resolution down to **500 ps** and a spatial resolution of **3.6 μm/pixel**.
- The resolution of each 4-Picos ICCD detector is **780 × 580 pixels** with a bit depth of **12 bits.**

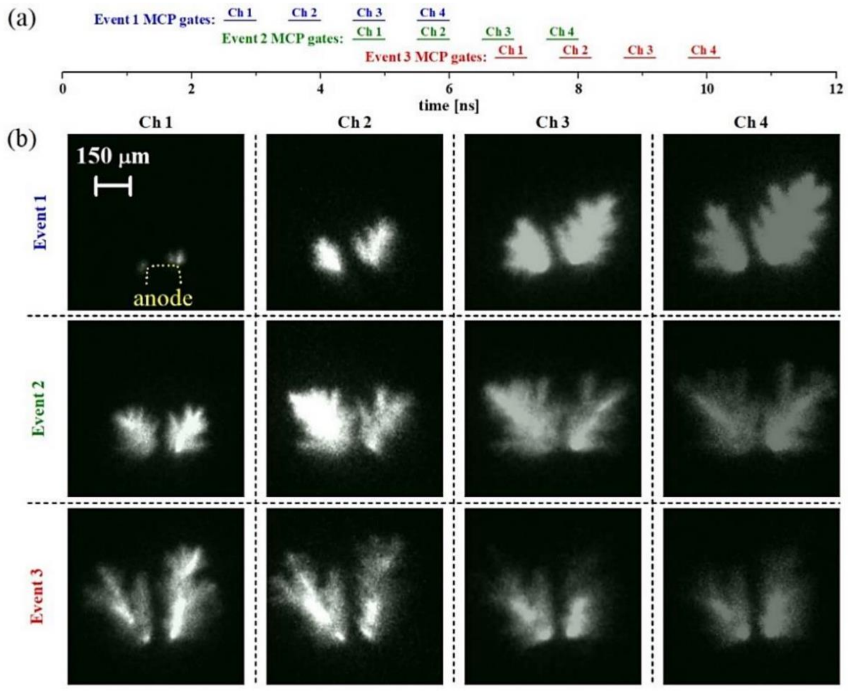

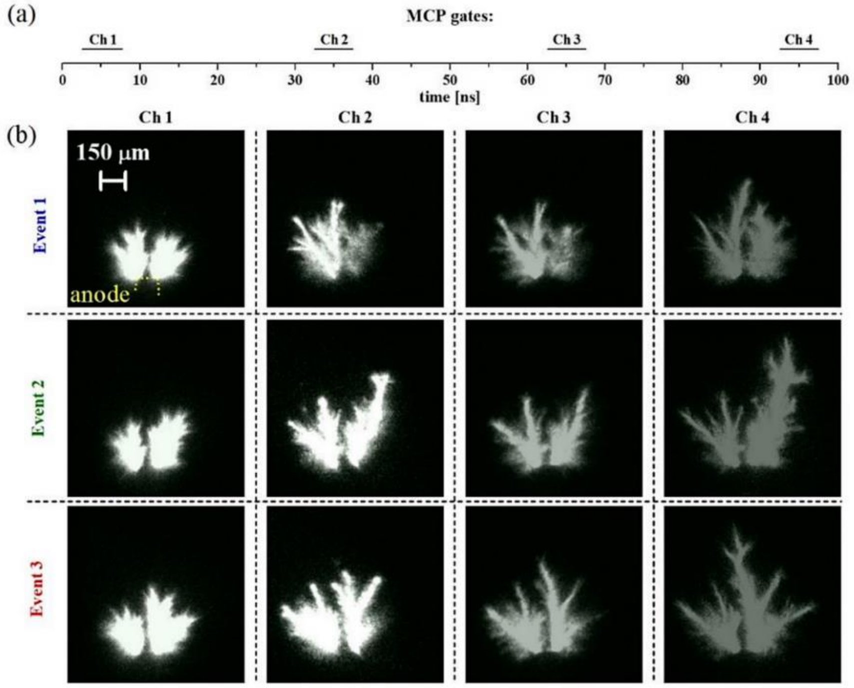

Prukner, V.; Schmidt, J.; Hoffer, P.; Šimek, M. Demonstration of Dynamics of Nanosecond Discharge in Liquid Water Using Four-Channel Time-Resolved ICCD Microscopy. Plasma 2021, 4, 183-200.

3. FOUR SYNCHRONIZED ICCD DETECTORS

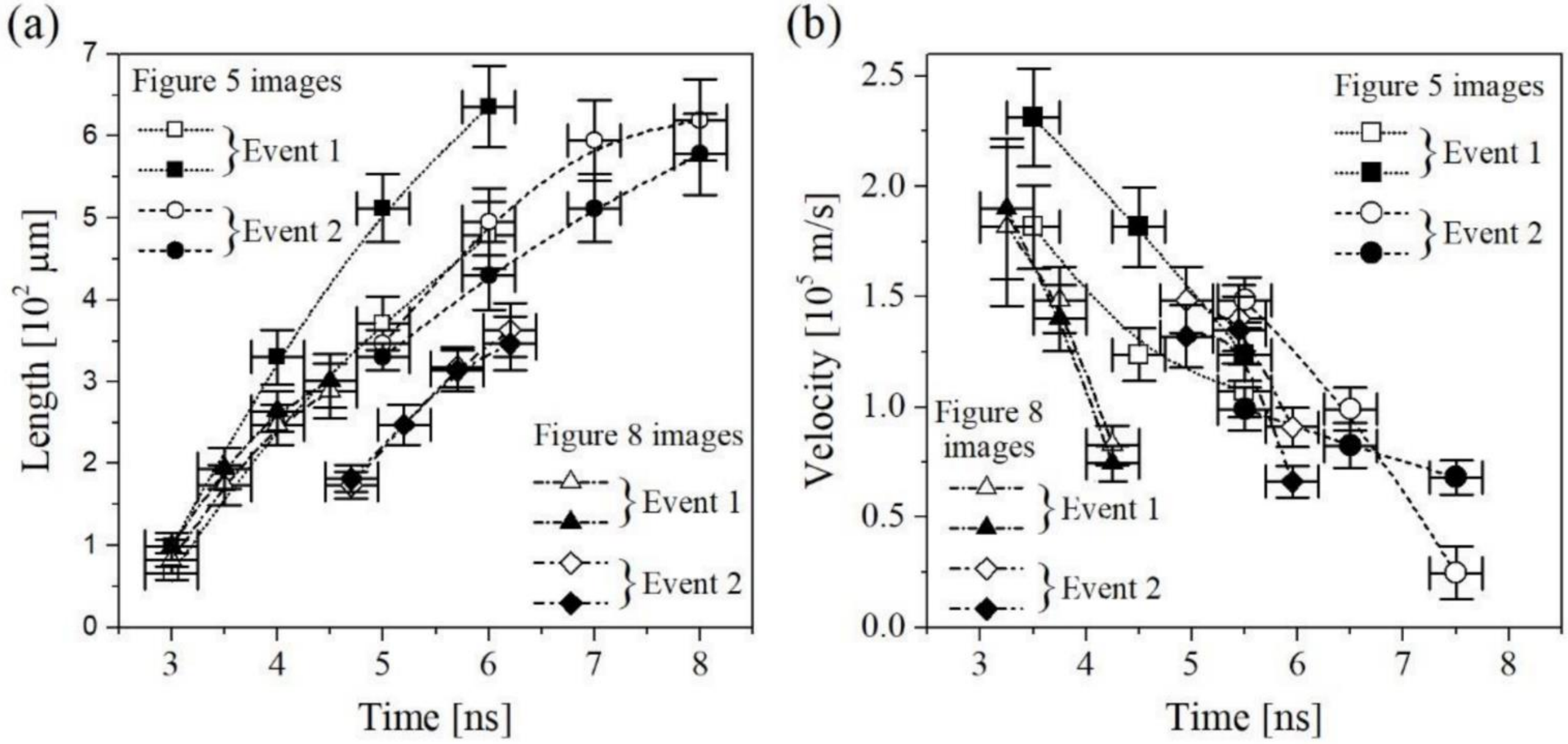

The highest expansion velocity is observed close to the anode tip during the first nanosecond of the discharge onset. The expansion then slows down with increasing distance from the anode tip until the growth of the filament stops during the descending slope of the HV pulse.

Prukner, V.; Schmidt, J.; Hoffer, P.; Šimek, M. Demonstration of Dynamics of Nanosecond Discharge in Liquid Water Using Four-Channel Time-Resolved ICCD Microscopy. Plasma 2021, 4, 183-200.

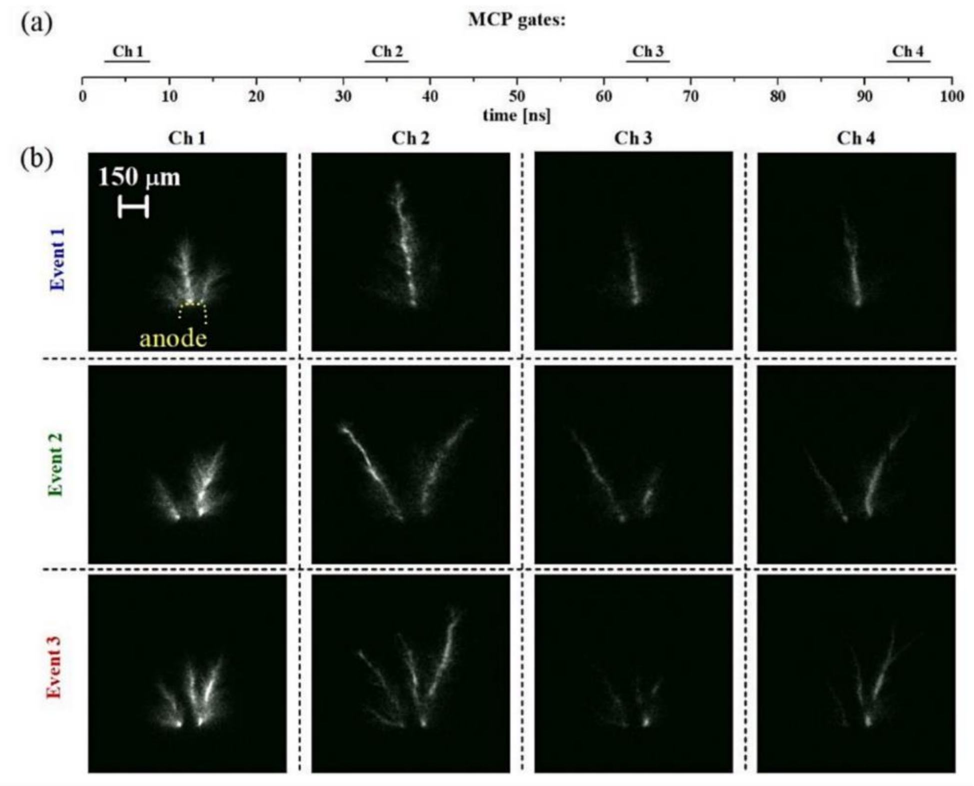

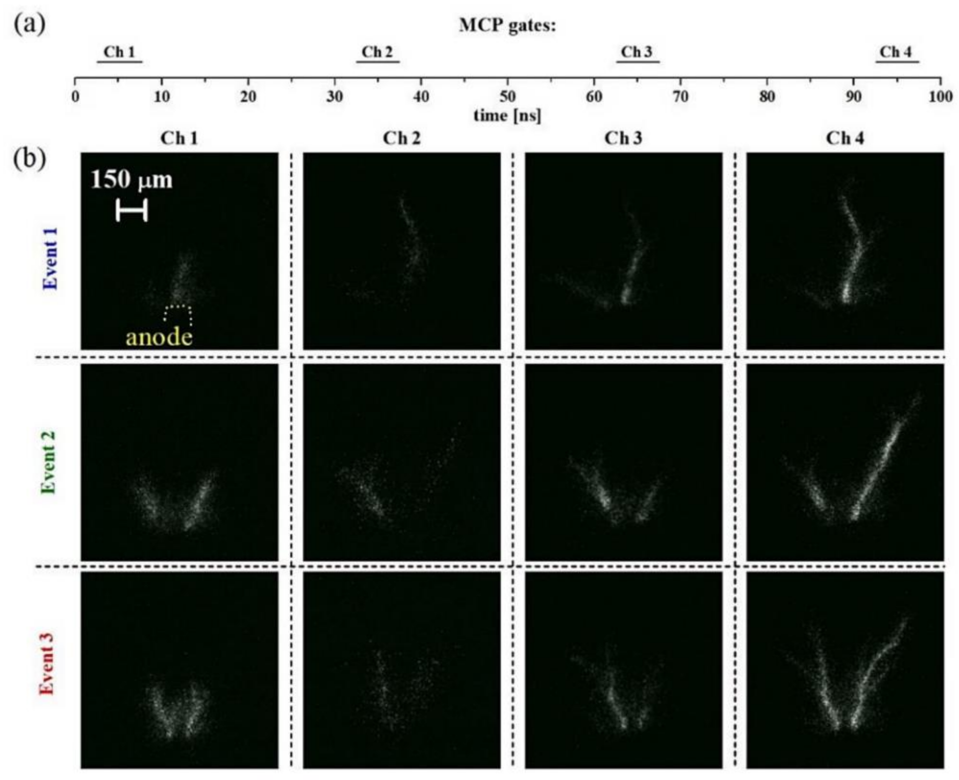

The entire branched filament maintains a homogeneous luminosity. **The dominant sources of the discharge luminosity are not predominantly localised on the moving luminous front, as in the case of classical ionising streamer fronts developing in gaseous dielectrics.**

Prukner, V.; Schmidt, J.; Hoffer, P.; Šimek, M. Demonstration of Dynamics of Nanosecond Discharge in Liquid Water Using Four-Channel Time-Resolved ICCD Microscopy. Plasma 2021, 4, 183-200.

4. PHANTOM HIGH-SPEED CAMERA

- Resolution **4 microns/pixel**
- Inter-frame delay of **10 microseconds**
- **Conditions of periodic discharge** (f=0.1 Hz)

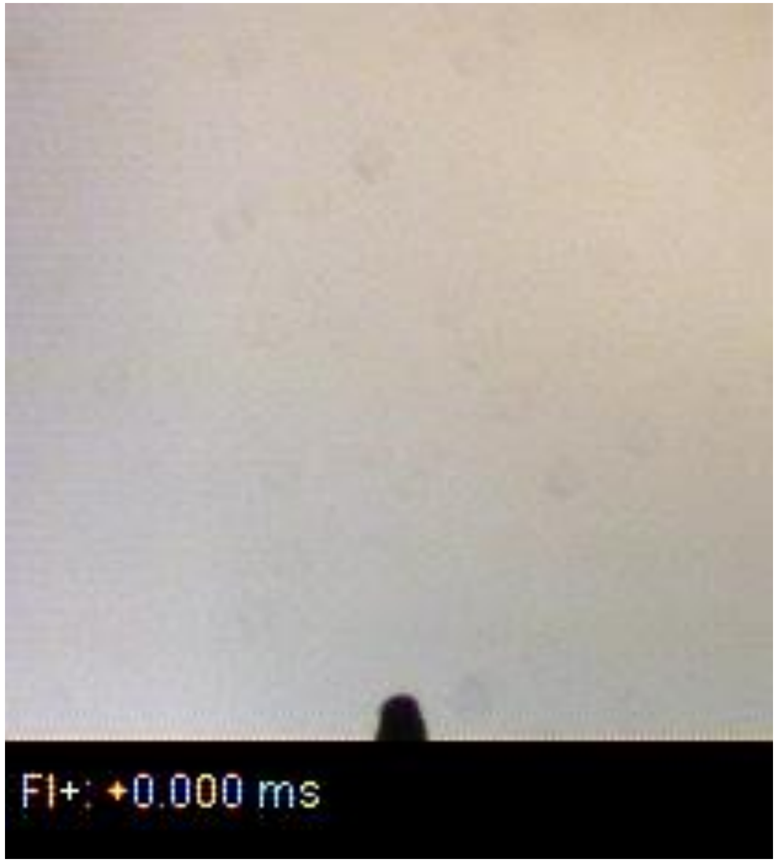

Petr Hoffer et al 2022 *Plasma Sources Sci. Technol.* 31 015005

4. PHANTOM HIGH-SPEED CAMERA

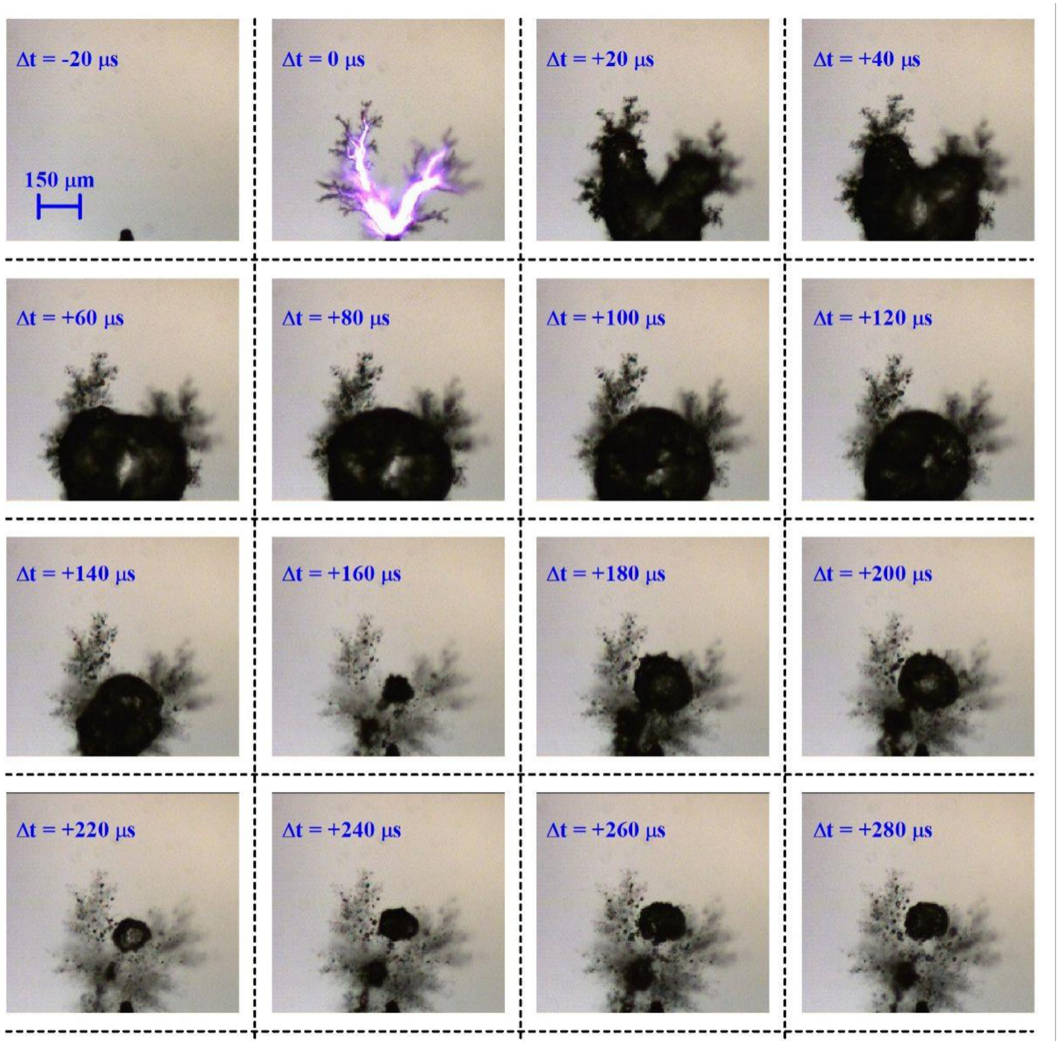

Process of formation and dissipation of gaseous macro-bubble formed around the tip of the anode from the discharge filaments as well as long-living micro-bubbles persisting close to the tip of the anode Acquired using discharge running periodically at a fixed repetition frequency of applied HV pulses (f = 0.1 Hz and HV amplitude of 145 kV on the anode side).

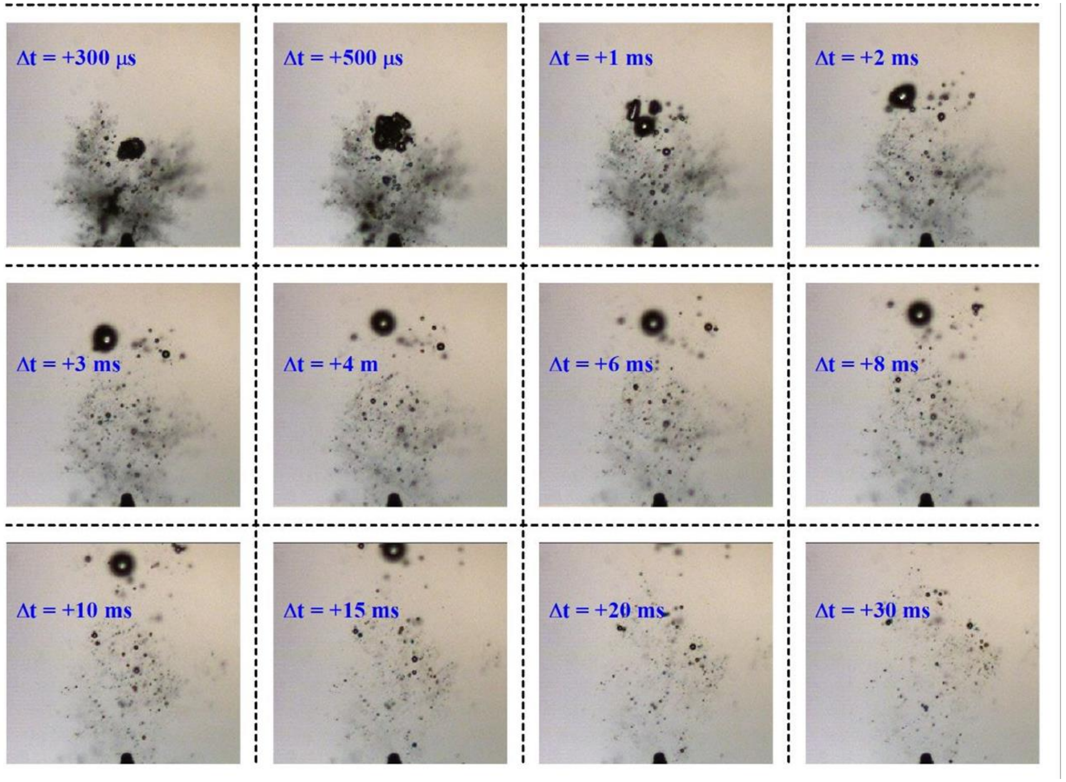

Petr Hoffer et al 2022 *Plasma Sources Sci. Technol.* 31 015005

Applied voltage pulse

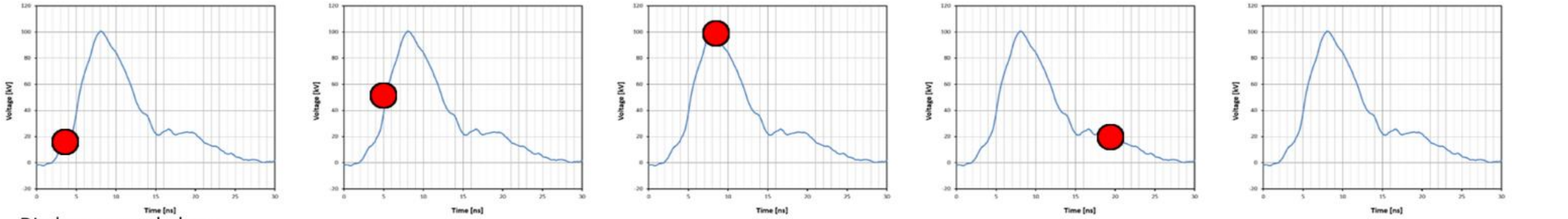

Discharge morphology

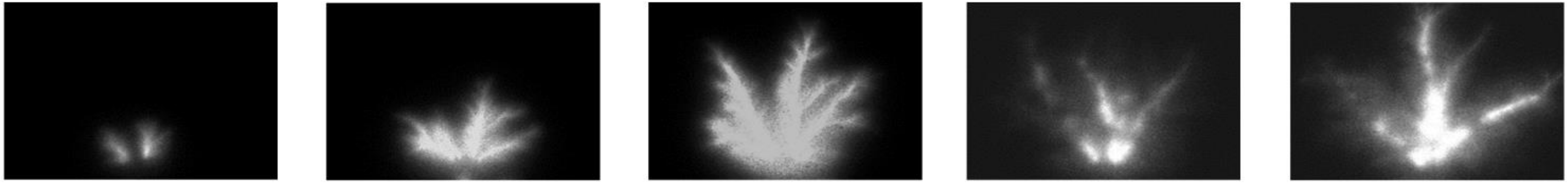

Emission spectra

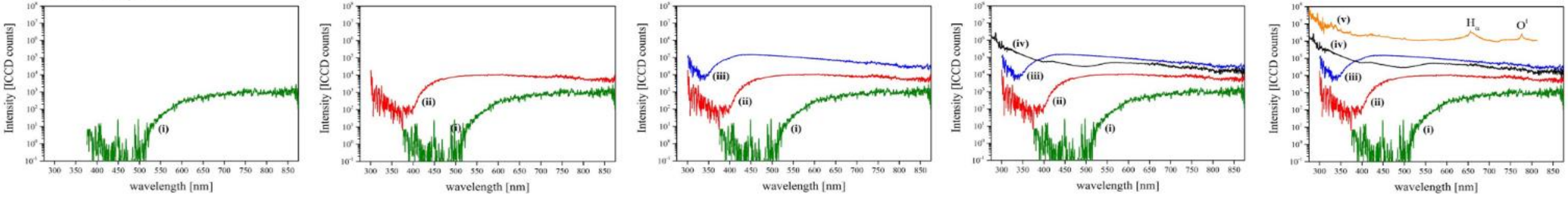

Milan Šimek *et al* 2017 *Plasma Sources Sci. Technol.* **26** 07LT01

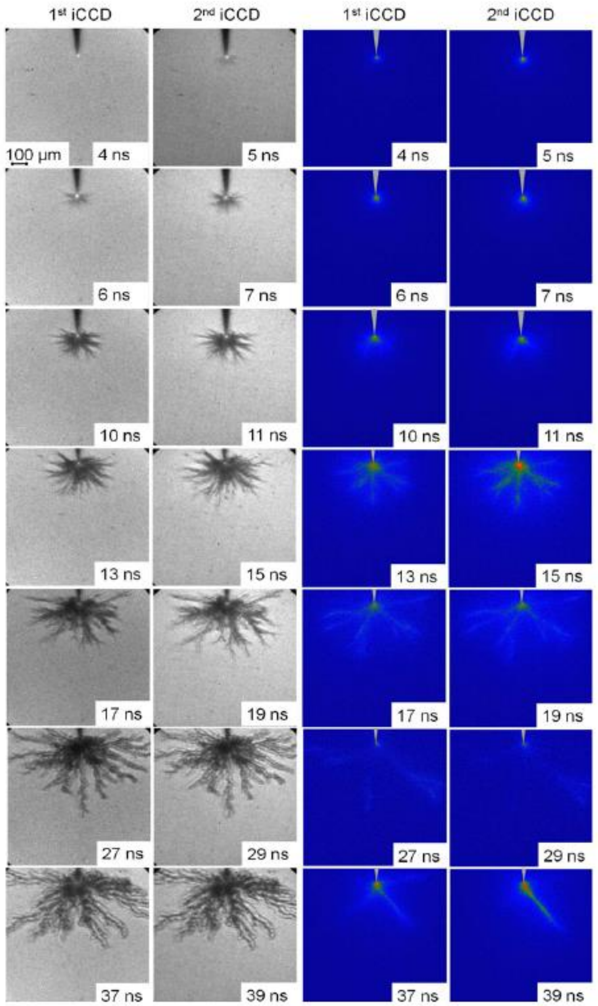

Figure 3. Shadowgraph and plasma emission visualization of a tree-like discharge in deionized water under 15 kV positive pulse with two synchronized iCCD cameras. This sequence is recorded during the first voltage pulse (see figure 1).

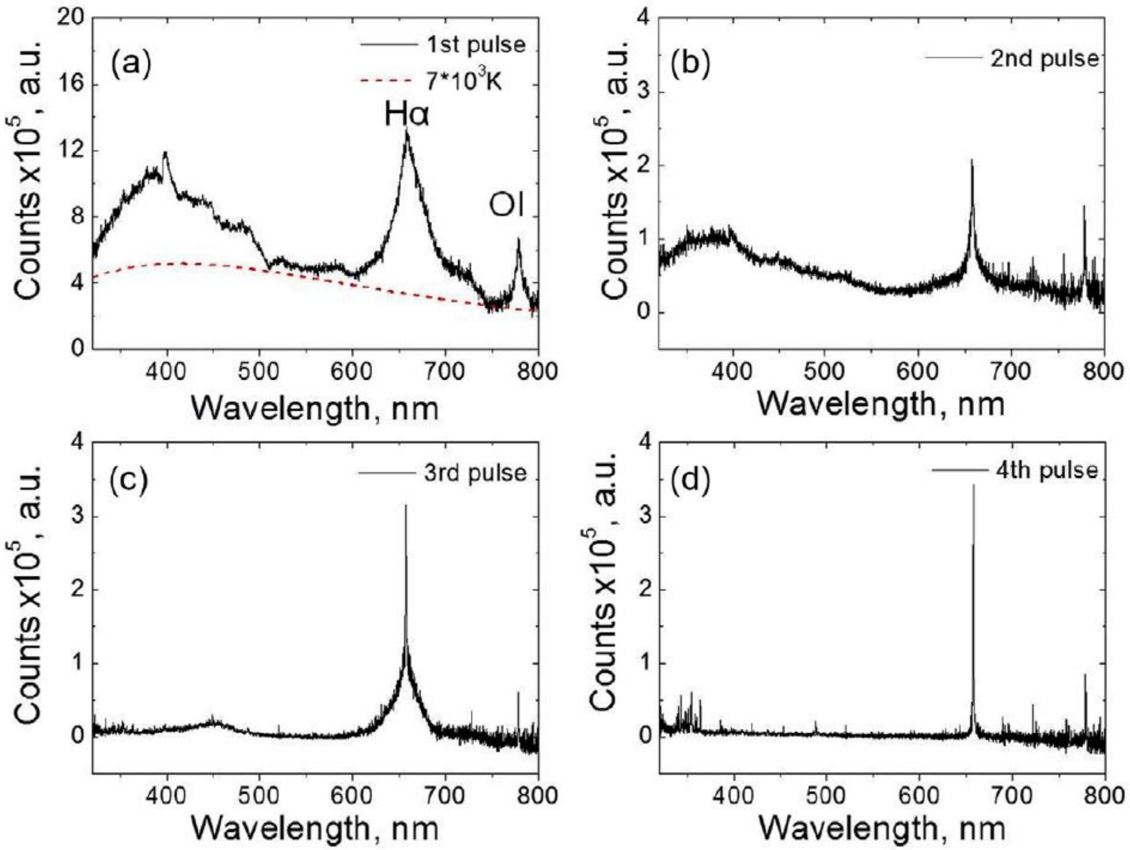

Figure 9. OES averaged over HV pulse duration corresponding to (*a*) first (positive), (*b*) second (negative), (*c*) third (positive) and (*d*) fourth (positive) pulses; deionized water at 15 kV.

Marinov et al, *J. Phys. D: Appl. Phys*. **47** (2014) 224017

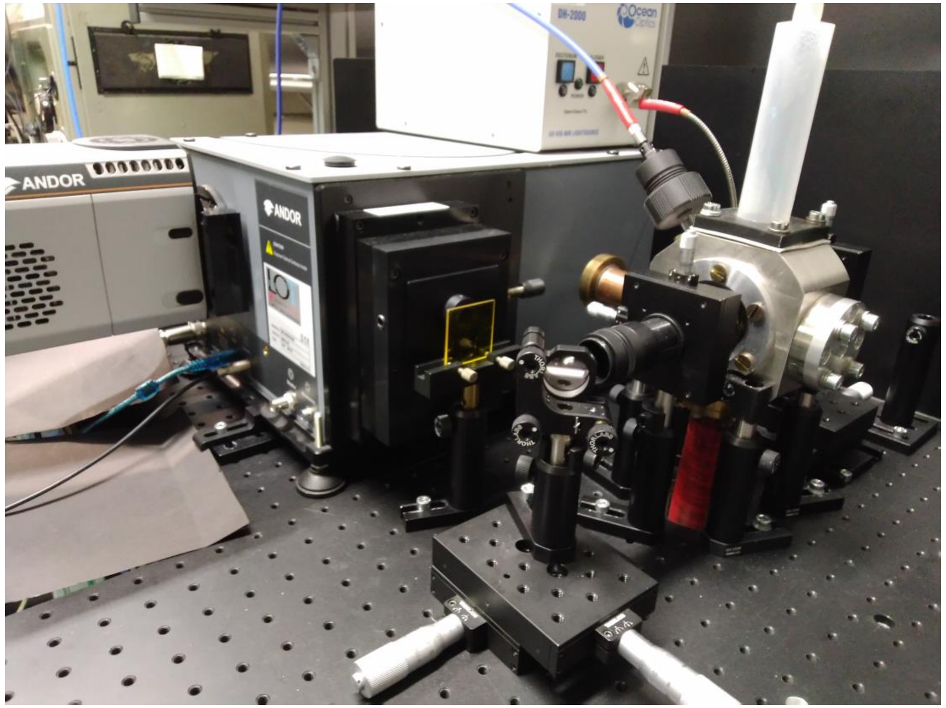

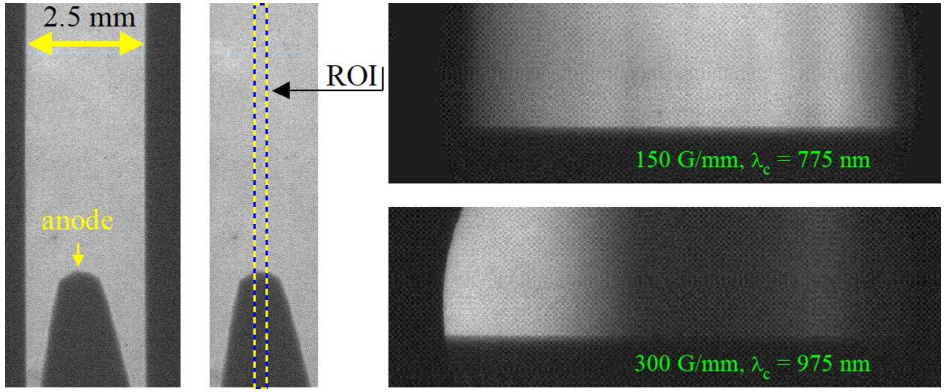

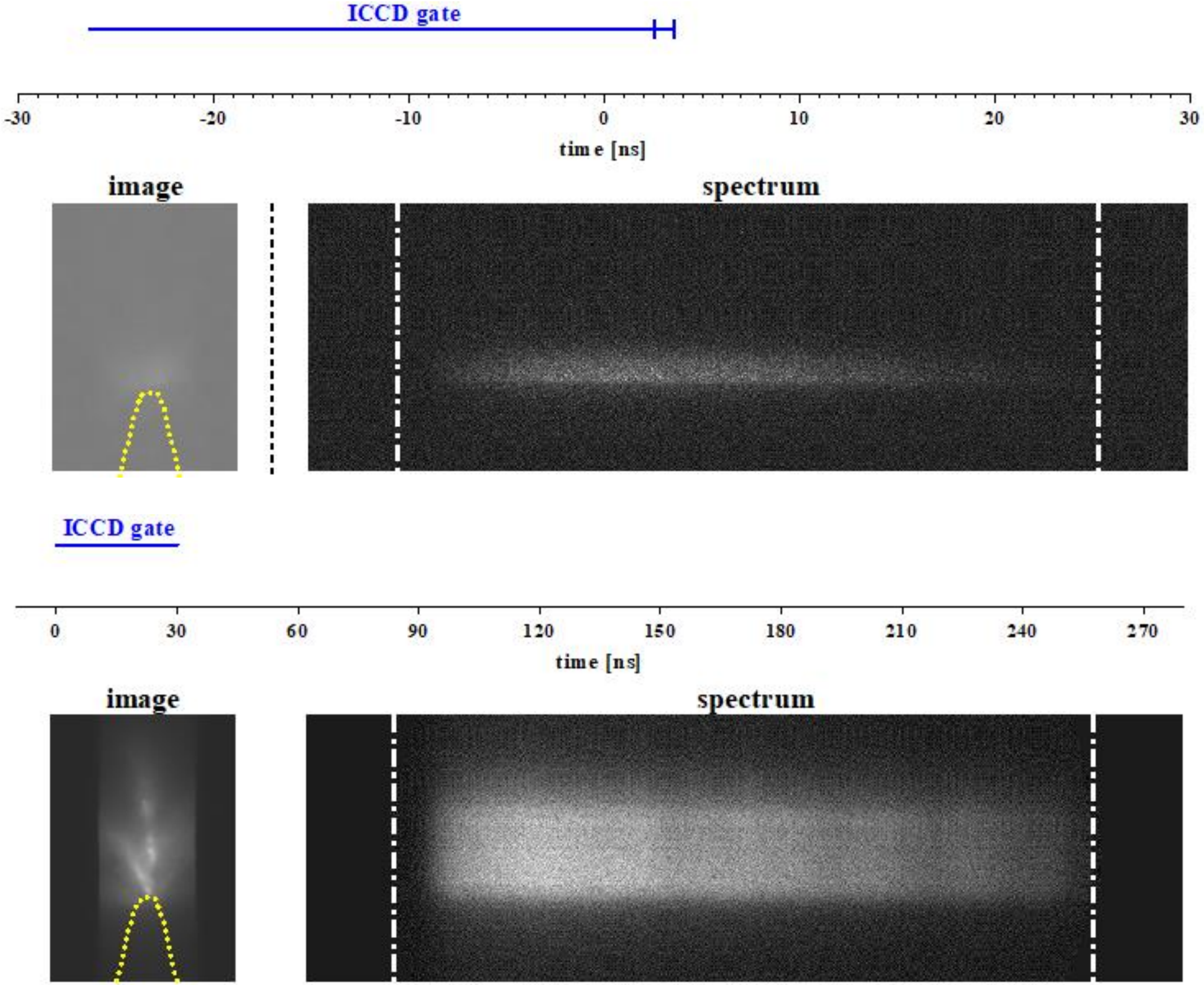

M. Simek et al 2022 work in progress

5. EMISSION SPECTROSCOPY

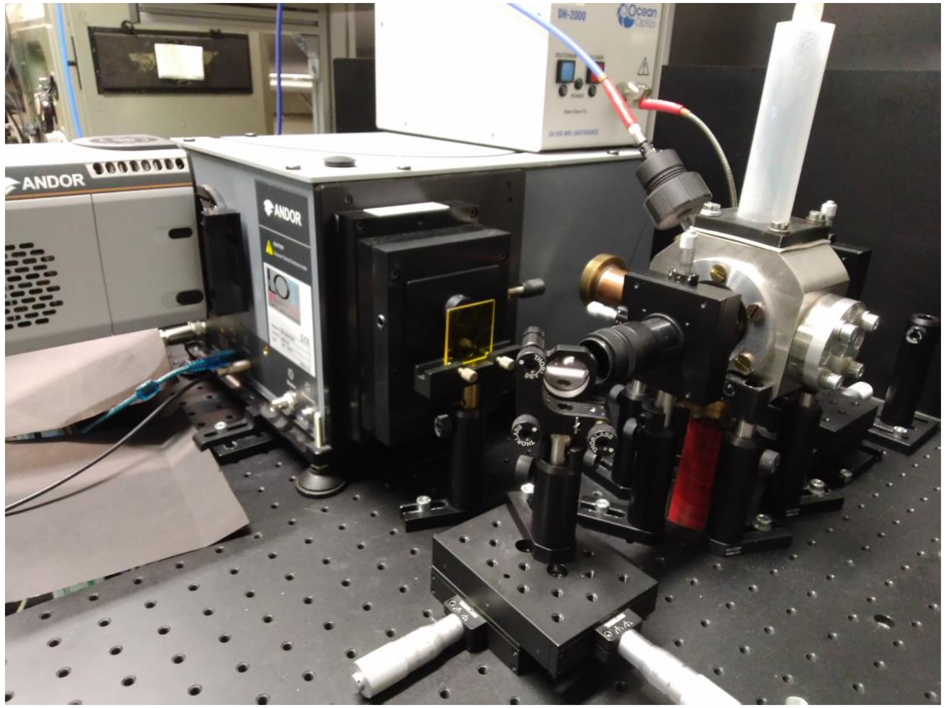

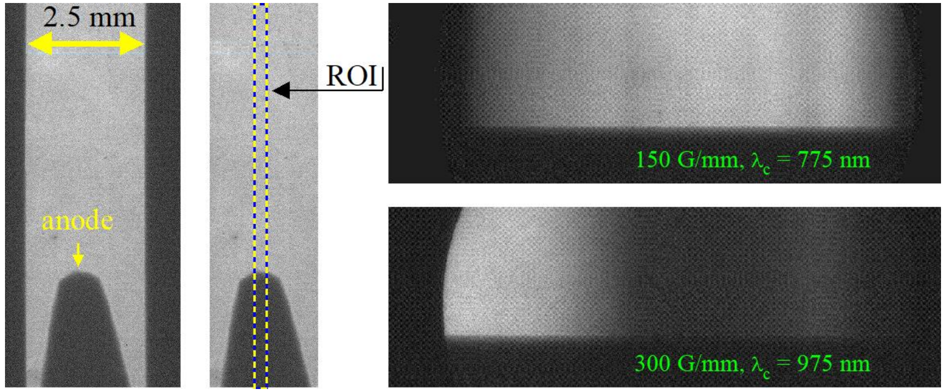

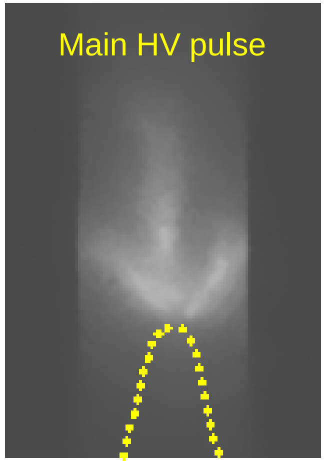

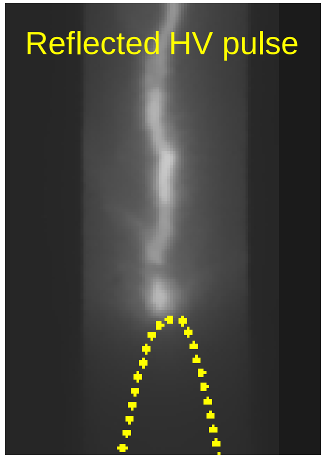

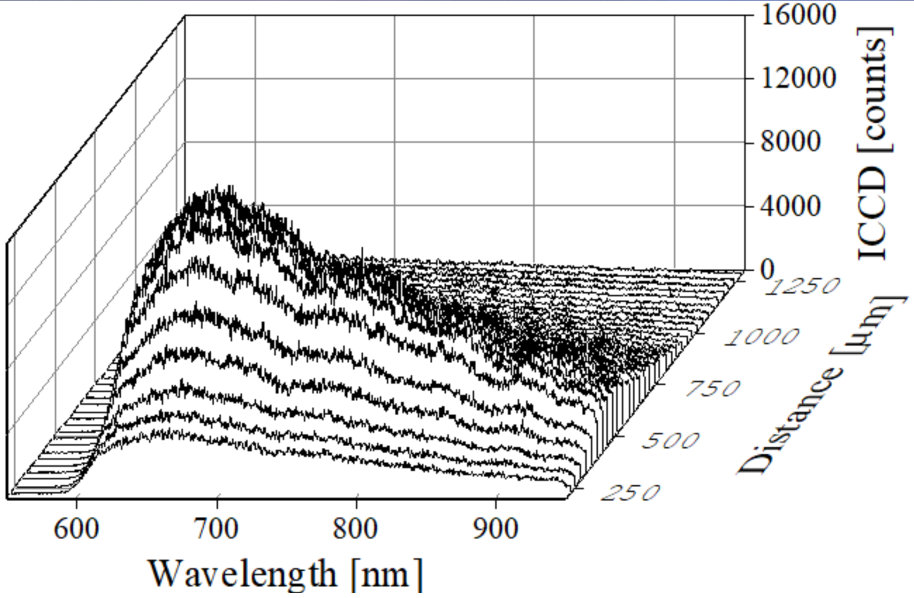

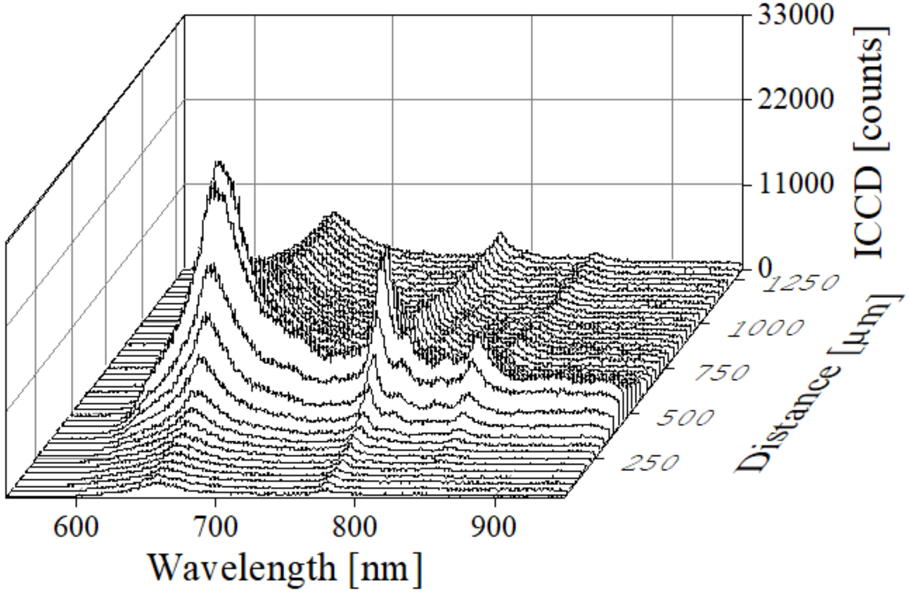

M. Simek et al 2022 work in progress

POSSIBLE EXPLANATION OF OBSERVED OPTICAL EMISSION

Bound – bound transitions :	$OH^+(A^3\Pi \rightarrow X^3\Sigma^-)$	322 - 422 nm
	$H_2O^+(\tilde{A}^2A_1 \rightarrow \tilde{X}^2B_1)$	380 - 480 nm
Bound – free transitions :	$H_2O(\tilde{C}^1B_1 \rightarrow \tilde{A}^1B_1)$	380 - 600 nm
	$H_2(a^3\Sigma_g^+ \rightarrow b^3\Sigma_u^+)$	120 - 600 nm
Free – free transitions :	$e + M \rightarrow e' + h\nu + M$	(Bremsstrahlung)

POSSIBLE EXPLANATION OF OBSERVED OPTICAL EMISSION

1. Autoionization (2 $H_2O \rightarrow H_3O^+ + OH^-$).
2. Detachment from OH^- on the interface of the water and the nanovoid.
3. Electron acceleration in nanovoid.
4. Electron H_2O collisions → bremsstrahlung

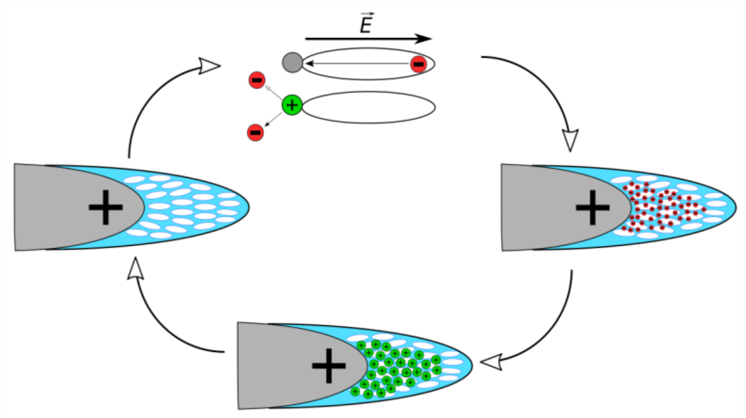

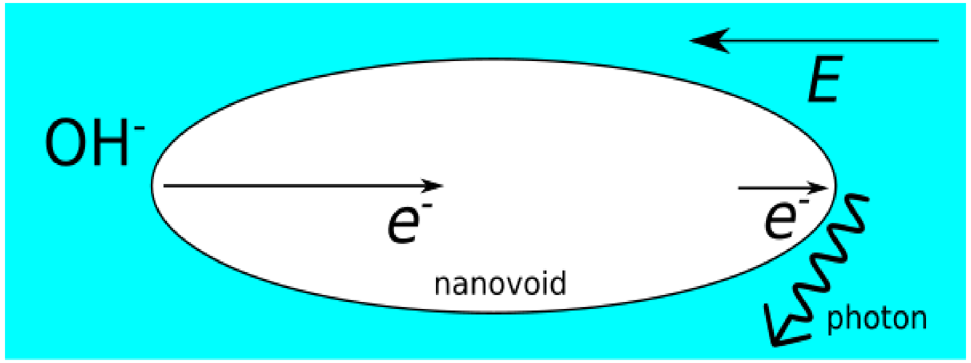

Moreover, the observed continua have sufficient energy to cause photodetachment from OH^-.

ZHANG and SHNEIDER 2021 *Journal of Applied Physics* **129** 103302

Ali Charchi Aghdam and Tanvir Farouk 2021 *Plasma Sources Sci. Technol.* **30** 065025

POSSIBLE EXPLANATION OF OBSERVED OPTICAL EMISSION

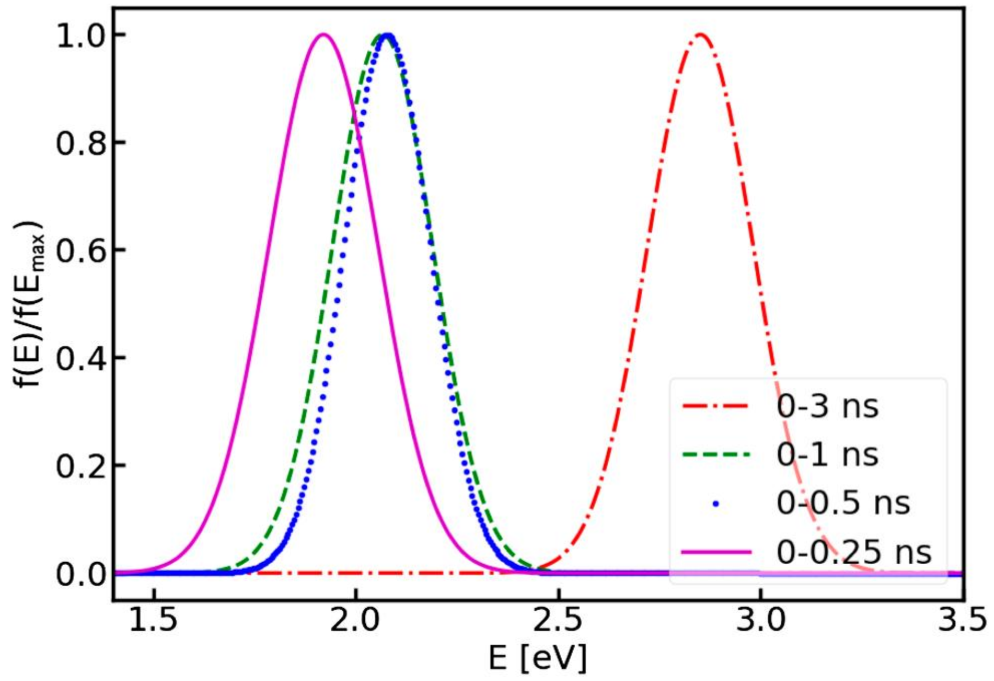

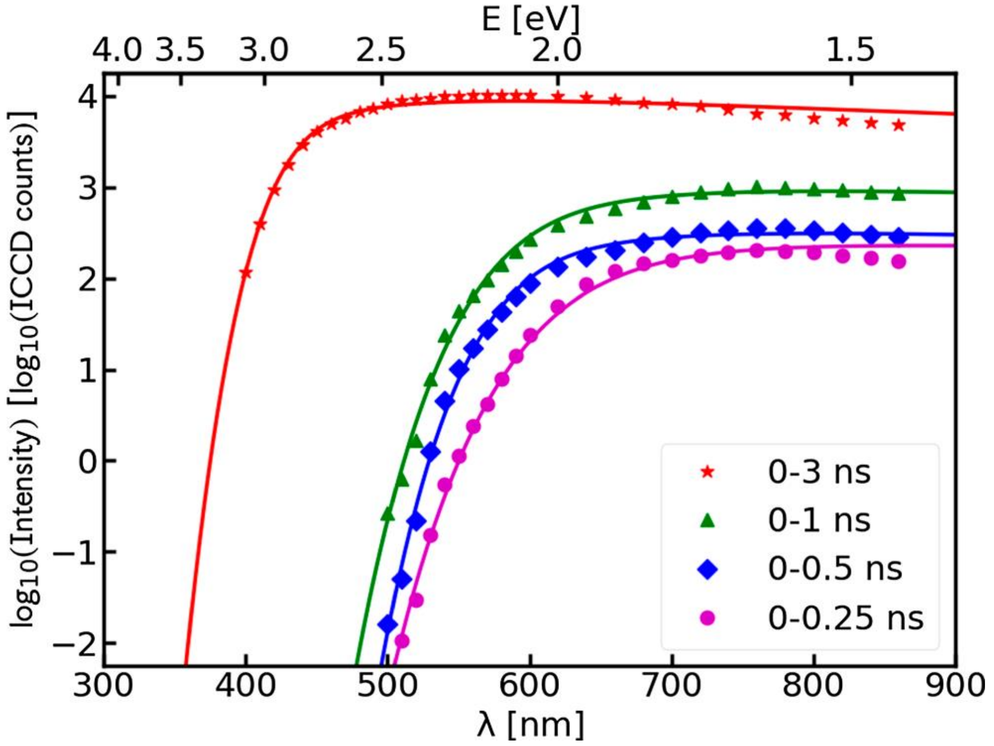

If we assume the following form of EEDF:

$$f(E) = A\exp\left(-\frac{(E-E_{\max})^2}{2\sigma^2}\right),$$

Emission coefficient of electron-neutral bremsstrahlung is:

$$\varepsilon_{\rm ff}^{\rm en} = \frac{\sqrt{\pi}}{2} C_{\rm en} \frac{n_{\rm e} n_{\rm n}}{\lambda^2} \int_{\frac{hc}{\lambda}}^{\infty} Q_{\rm en}^{\rm m} \left(1-\frac{hc}{2\lambda E}\right)\sqrt{1-\frac{hc}{\lambda E}}\, E^{\frac{3}{2}} f(E)\,{\rm d}E \ [\mathrm{W\ m^{-4} sr^{-1}}],$$

$$I(\lambda) = \frac{K}{\lambda^2}\int_{\frac{hc}{\lambda}}^{E_\infty} Q_{\rm en}^{\rm m}(E)\left(1-\frac{hc}{2\lambda E}\right)\sqrt{1-\frac{hc}{\lambda E}}\times$$
$$\times E^{\frac{3}{2}} \exp\left(-\frac{(E-E_{\max})^2}{2\sigma^2}\right){\rm d}E.$$

Petr Bílek *et al* 2021 *Plasma Sources Sci. Technol.* **30** 04LT01

SUMMARY

- The direct ns discharge in liquid water develops through a sequence of dark and luminous phases characterized by a very rapid initial expansion of the discharge area, followed by the collapse of the discharge.
- **The presence of the luminous phase implies the prior occurrence of the dark phase.** The dark filaments start occurring with a delay of **~3–4 ns** after the onset of the HV pulse and subsequently expand at velocity of **$\sim 1\times10^5$–2×10^5 ms^{-1}** and the luminous discharge phase is delayed by **~600–800 ps** with respect to the onset of the dark filaments.
- Observed shock-fronts (produced by individual filaments) are characterized by peak pressures between 0.4 and 12 GPa. **It is worth noting that the strongest shock-fronts (6-12 GPa) are regularly associated with the dark filaments containing strong residual PIE (originated from the subsequent luminous phase).**
- Exclusive spectrometric fingerprints characterizing ‘direct’ breakdown seem to be the bound-free and free-free transitions (no atomic H/O lines). **Electron–neutral bremsstrahlung** radiation seems to be good candidate to explain the initial emission spectra.
- Bound – bound (atomic) emission (by hydrogen and oxygen) occurs later (during discharges initiated by reflected HV pulses **and most likely in the presence of a gas phase**).
- Temporal and spatial resolution matters (sub-nanoseconds & few micrometers) !

KEY MESSAGE TO BE LEARNED

- **To study a direct ns discharge in liquid water with all related phenomena, a good starting point is to check whether the studied liquid does not contain (micro)bubbles.**

- **Experimental approaches based on averaging data acquired from events produced under periodic discharge conditions should be avoided.**

- **Experimental results obtained under single pulse conditions in degassed water appear to be compatible with the qualitative picture based on the initial and abrupt perturbation in liquid water integrity caused by electrostriction followed by acceleration and multiplication of electrons in low density regions and subsequent development of the discharge through luminous branched filaments.**

Outlook

- **Spatially-resolved nanosecond ICCD spectrometry – extension of the spectral range (200 -1000 nm)**
- **Electro-optical/emission characteristics of the discharge in water saturated by microbubbles (burst regime)**
- **Other laser based techniques (SRS, DLS, …)**

Project & Funding GAČR 18-04676S

GAČR GRANTOVÁ AGENTURA ČESKÉ REPUBLIKY

Petr Hoffer[1], Petr Bílek[1], Václav Prukner[1], Jiří Schmidt[1] and Milan Šimek[1]
Petr Bílek[2], Ján Tungli[2], Tomáš Hoder[2] and Zdeněk Bonaventura[2]

[1]Institute of Plasma Physics of the Czech Academy of Sciences, Prague, Czech Republic
[2]Department of Physical Electronics, Faculty of Science, Masaryk University, Brno, Czech Republic

Relevant papers:

- Šimek M., Hoffer P., Tungli J., Prukner V., Schmidt J., Bílek P., Bonaventura Z.: **Investigation of the initial phases of nanosecond discharges in liquid water**. *Plasma Sources Science & Technology* **29** 6 (2020) 064001
- Šimek M., Hoffer P., Prukner V., Schmidt J.: **Disentangling dark and luminous phases of nanosecond discharges developing in liquid water**. *Plasma Sources Science & Technology* **29** 9 (2020) 095001
- Prukner V., Schmidt J., Hoffer P., Šimek M.: **Demonstration of Dynamics of Nanosecond Discharge in Liquid Water Using Four-Channel Time-Resolved ICCD Microscopy**. 4 (2021) 183-200
- Bonaventura Z., Tungli J., Bílek P., Šimek M.: **Electron multiplication and avalanching in nanovoids at the initial stage of nanosecond discharge in liquid water**. *Plasma Sources Science & Technology* **30** 6 (2021) č. článku 065023
- Hoffer P., Prukner V., Schmidt J., Šimek M.: **Shockwaves evolving on nanosecond timescales around individual micro-discharge filaments in deionised water**. *Journal of Physics D: Applied Physics* **54** 28 (2021) 285202
- Bílek P., Tungli J., Hoder T., Šimek M., Bonaventura Z.: **Electron–neutral bremsstrahlung radiation fingerprints the initial stage of nanosecond discharge in liquid water**. *Plasma Sources Science & Technology* **30** 4 (2021) 04LT01
- Hoffer P., Bílek P., Prukner V., Bonaventura Z., Šimek M.: **Dynamics of macro- and micro-bubbles induced by nanosecond discharge in liquid water**. *Plasma Sources Science & Technology* **31** 1 (2022) č. článku 015005
- Bonaventura Z., Bílek P., Tungli J., Šimek M.: **Analysis of secondary emission mechanism in electron avalanches propagating in cylindrical nanoruptures in liquid water**. *Plasma Sources Science & Technology* **31** 3 (2022) č. článku 035003

THANK YOU